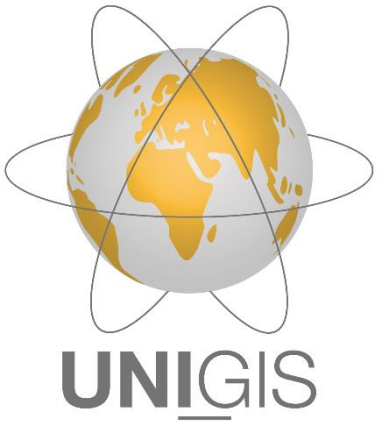

Master Thesis

submitted within the UNIGIS MSc programme
Department of Geoinformatics - Z_GIS
University of Salzburg

Assessing the applicability of Sentinel-1 SAR data for semi-automatic detection of snow avalanche debris

by

Mattia Sartori, BSc
106939

A thesis submitted in partial fulfilment of the requirements of
the degree of
Master of Science (Geographical Information Science & Systems) – MSc (GI Sc)

Advisor:
Dr. Zahra Dabiri

Trento, 12.04.2023

Acknowledgments

I would like to thank Zahra Dabiri for guiding me through the creation of this work, from the conceptualisation of the first ideas, all the way through the writing process. Her willingness and availability to provide support in every phase have been inestimable. I also want to thank the whole UNIGIS team for the support showed during the MSc program that led to the creation of this final work.

This master's Thesis would not have been achievable without the regional departments of avalanche forecast and prevention, namely Meteotrentino and Amt für Meteorologie und Lawinenwarnung. Special thanks also go to the Austrian Lawinenwarndienst and to the valuable time that the avalanche expert Dieter Blümel dedicated to meticulously inspect and judge single avalanche events.

I am also truly thankful to Ulisses Sosa for providing support in passages that required a deeper knowledge of the Phyton programming language, Alvise Sartori and Caterina Sartori for proofreading the manuscript.

Finally, I would like to thank my family, Rebecca and Elias for the support and patience dedicated to me, and for the time they made available to create this work, and to cover the whole MSc journey.

Acronyms

ARD	Analysis Ready Data
ASF	Alaska Satellite Facility
CNN	Convolutional Neural Networks
CRS	Coordinate Reference System
DAAC	Distributed Active Archive Centers
dB	Decibel
DEM	Digital Elevation Model
ESA	European Space Agency
EAWS	European Avalanche Warning Services
GIS	Geographic Information System
GRD	Ground Range Detected
HR	High Resolution
ISO	Iterative Self Organizing
IW	Interferometric Wide
LiDAR	Light Detection and Ranging
MSI	Multispectral Instrument
NRB	Normalized Radar Backscatter
OBIA	Object Oriented Image Analysis
PPV	Positive Predictive Value
PRA	Potential Release Area
RGB	Red, Green, Blue
RTF	Radiometric Terrain Flattening
SAR	Synthetic Aperture Radar
SNAP	Sentinel Applications Platform
TauDEM	Terrain Analysis Using Digital Elevation Models
TOPSAR	Terrain Observation with Progressive Scanning SAR
UTM	Universal Transverse Mercator
VAE	Variational Autoencoder
VH	Vertical-horizontal (polarisation)
VV	Vertical-vertical (polarisation)
WGS	World Geodetic System
σ0	Sigma Nought
β0	Beta Nought
γ0	Gamma nought

Science pledge

I hereby declare that the thesis is entirely the result of my work. I have cited all sources I have used in my thesis, and I have always indicated their origin. This thesis was not previously presented to another examination board and has not been published.

Place, Date: Trento, 12/04/2023 signature: 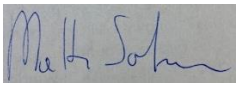

Abstract

Snow avalanches are catastrophic natural disasters that threaten the safety of people and infrastructure causing casualties and damage yearly, in all populated mountain regions of the world. When infrastructure is damaged, these events can also lead to major economic loss. Prevention is currently based on a daily avalanche bulletin that informs the population about the snowpack stability, assigning a danger level on a scale from one to five. Essential information about the spatial distribution and size of avalanches, aimed at mitigation measures, hazard mapping and forecasting, is incomplete or absent at present. Such knowledge about the spatial and temporal occurrence of avalanche activity is critical for hazard mapping and forecasting, and could be integrated in the current prevention system. Long-term avalanche monitoring over large regions can best be achieved using a spaceborne synthetic aperture radar (SAR) system offering all weather, day and night operation, with broad coverage, which ensures data continuity. This study aims to assess the applicability of Sentinel-1 SAR data to semi-automatically detect avalanche debris in the western part of the Italian region of Trentino-South Tyrol using the snow rich period of winter 2017-2018 as a reference. Utilizing SAR data, avalanches were detected by identifying changes in backscatter caused by the rough snow surface created by the debris deposited in the avalanche's runout zone. Detection is performed by creating and comparing image pairs consisting of an active Sentinel-1 SAR image (where avalanches are potentially present) with a baseline Sentinel-1 SAR image taken twelve days previously. By using both Sentinel-1 A & B, the temporal baseline was reduced to six days. Change detection techniques and unsupervised object-based classification were applied to detect new avalanche debris. Results show that 65% of avalanches were correctly detected and those not detected are located within forested areas or on agricultural land where Sentinel-1 SAR signals might have been disturbed, due to the temporal decorrelation of six days. Further investigation would be required to assess the applicability of the proposed model on a regional scale, especially focusing of its accuracy by comparing the results to a broader set of reference data, which was limited in this study. This research has been accepted to be presented at the 2023 International Forum for Geoinformatics in Salzburg and is currently being reviewed to be published in the GI_Forum Journal issue 2.

Keywords:

Sentinel-1 SAR, Unsupervised Object Classification, Change Detection, Avalanche Debris

Contents

Acknowledgments i
Acronyms ii
Science pledge iii
Abstract iv
Contents v
List of Figures vi
List of Tables vii
Introduction 1
Background 1
Radar backscatter physics of snow 3
Avalanche mapping using remote sensing 4
Problem definition 5
Aims and objectives 6
Materials / Methods 7
Investigation Area 7
Data 8
Sentinel-1 SAR data 9
Mapped avalanches 12
Miscellaneous data 15
Workflow 17
Pre-processing 18
Masks 20
Manual avalanche detection 24
Change detection 25
Classification 26
Validation process 28
Results 29
Masks 29
Change detection 32
Semi-automatically detected avalanches 35
All detected avalanches 37
Comparison with mapped avalanches 39
Comparison with manually detected avalanche debris 40

False positives 43
Discussion 45
Limitations 46
Conclusion 50
Outlook 51
References 53

List of Figures

Figure 1: The Trentino-Alto Adige region of interest with the investigation area highlighted in green. 8

Figure 2: Snow avalanche taken as example to show the subdivision into zone of origin, where the avalanche is triggered; zone of transition and zone of deposition where snow runs out and produces a rough surface (Figure adopted from Leinss et al. 2020). 11

Figure 3: Mapped avalanches available as reference data for the South Tyrol region (above) and the Trentino (below) region. In Trentino avalanches have no specification about the event date, accordingly they fall into the category “avalanches other years” 14

Figure 4: General workflow employed to process Sentinel-1 SAR data in order to obtain clusters of possible avalanche debris. 17

Figure 5: The four layers of masked-out areas for which analysis was not performed due to the unlikelihood of avalanche debris to be deposited. 20

Figure 6: Binary map that partitions the investigation area into zones of possible runout, and zones where runout is not expected. 23

Figure 7: In green area of shadow and layover. (A) highlights the western border of the investigation areas where areas of shadow and layover are widespread to a greater extent. (B) shows a detail of a mountain group (Brenta) with particularly high and steep mountainous formations. 30

Figure 8: (Left) areas that fall outside avalanche runout zones (No Runout) are excluded from analysis together with (right) forested and urban areas. 31

Figure 9: Map series showing (top left) the mapped Sattel avalanche in red with the expected zone of deposition in yellow; (top right) the change detection image created from VH polarisation; (centre left) application of a high pass filter; (centre right) application of a low pass filter; (bottom left) application of a refined lee filter; (bottom right) application of a median filter. .. 33

Figure 10: Map series showing (top left) the mapped Sattel avalanche in red with the expected zone of deposition in yellow; (top right) the change detection image created from VV polarisation; (centre left) application of a high pass filter; (centre right) application of a low pass filter; (bottom left) application of a refined lee filter; (bottom right) application of a median filter. .. 34

Figure 11: An avalanche event dating from 25.01.2018 in the upper Schnals valley (South Tyrol) that was partially detected using SAR data. The detected avalanche debris (yellow) cover less than 50% of the expected zone of deposition, making this a partially detected avalanche. 35

Figure 12: An avalanche event dating from 25.01.2018 in the upper Schnals valley (South Tyrol) that was partially detected using SAR data. The detected avalanche debris (yellow) cover less than 50% of the expected zone of deposition, making this a partially detected avalanche. 36

Figure 13: All semi-automatically detected avalanches of the season, sub-divided into detections from co-polarized VV data and cross-polarized VH data. 38

Figure 14: Out of all mapped avalanches on the selected date, 44% were totally detected using SAR data, 19% were partially detected, and 37% were missed. 40

Figure 15: The boundaries of a mapped avalanche (left), RGB image composite showing in green increased backscatter values in VH polarisation (centre), and in VV polarisation (right). 41

Figure 16: Avalanche debris polygon likely to be a false positive. 44

List of Tables

Table 1: All queried Sentinel-1 SAR scenes from Sentinel-1 A&B satellites (S1A, S1B), Interferometric Wide (IW) acquisition mode, Ground Range Detected High Resolution (GRDH) products. 10

Table 2: Mapped avalanches availability divided for the two regions of interest. 13

Table 3: amount of fresh snow registered at two selected meteorological stations for the two regions of interest. Only days with a considerable amount of precipitation were chosen and displayed. 16

Table 4: Description and chosen values of the parameter that can be fine tuned before executing the Potential Release Area (PRA) algorithm. 21

Table 5: SAR scenes deleted due to the lack of avalanche events caused by the absence of a relevant snow cover. 36

Table 6: Detected avalanche debris patches for every SAR scene, sub-divided into VV polarisation and VH polarisation. 37

Table 7: Mapped avalanches on selected days, detected avalanches resulting from the semi-automatic detection method, and rate of correctly detected avalanches. 39

Table 8: Number of avalanches manually detected by the author, and number of avalanches confirmed by the expert. 40

Table 9: Avalanches that were correctly detected with the semi-automatic approach compared with manually mapped avalanches from SAR RGB composite images. 41

Introduction

A snow avalanche (hereinafter "avalanche") is a snow mass that rapidly descends steep slopes. It can also contain rocks, ice, vegetation or soil (Schweizer, Bruce Jamieson and Schneebeli, 2003). Based on their release type, avalanches can be divided into loose snow avalanches and slab avalanches. Loose snow avalanches start from areas characterized by a small volume cohesionless surface layer of wet or dry snow. They increase in size while descending but tend to affect only the top layers of snow, thus remaining usually smaller and less dangerous. In comparison, slab avalanches involve the release of a cohesive slab that can extend over a large plane and reach much more destructive force due to their mass (McClung, 2002). A slab avalanche can be triggered by different factors such as localized loading by people or explosives (called artificial triggering), or gradual uniform loading due to precipitation, or a no-loading situation that changes the proprieties of the snowpack due to surface warming (called natural triggering or spontaneous release) (Schweizer, Bruce Jamieson and Schneebeli, 2003).

This research focuses on the identification of an avalanche's **zone of deposition**, which refers to the bottom accumulation zone where snow debris piles after snow masses lose the momentum produced by the sliding process and stop. The type of avalanche will, therefore, not be taken into consideration when performing semi-automatic detection as the zone of origin (the starting point of an avalanche) is not the focus of this study. Nevertheless, avalanches detected by the proposed model can be both slab avalanches and loose snow avalanches.

Background

An avalanche is a major natural disaster that seriously threatens the safety of inhabitants, socioeconomic development and biodiversity (Yang *et al.*, 2020). Between 2018 and 2022, snow avalanches caused the death of 347 people, with 129 casualties in the winter season 2020-2021 alone in Europe (EAWS, 2023b). When accounting for infrastructure damage and loss caused by general mobility restrictions, it is difficult to quantify the economic harm caused by these events. Nonetheless, based on studies on the damage potential of avalanches it is clear that economic loss plays a major role in the repercussion of avalanches on society in general (Keiler *et al.*, 2005). Especially in densely populated mountainous regions, these events can be extremely destructive and catastrophic, endangering people and infrastructure (Yang *et al.*, 2020).

Forecasting, and thus avoiding exposure to avalanches, is currently the most important measure to mitigate hazards and it consists in predicting the current and future snow instability in space and time (McClung, 2002). In the Alps, forecasting is implemented

through a warning bulletin issued daily over the winter months that informs the population about the current danger level that can range from low (1), moderate (2), considerable (3), high (4) and very high (5) (Wesselink *et al.*, 2017). In Europe, these danger levels are centrally defined by the European Avalanche Warning Services (EAWS, 2023a) and applied locally by regional offices, e.g. the "avalanche report" project that unites bulletins from three states/provinces (Euregio, 2022). The avalanche danger scale that defines danger levels is a function of snowpack stability, the frequency distribution of snowpack stability, and avalanche size for a given unit of area and time (EAWS, 2023a). Snow stability is inferred by experienced avalanche professionals based on the knowledge about triggering meteorological factors, terrain and sparsely available snowpack observations (Chawla and Singh, 2021). Sufficient snow stability data for accurate forecasting is generally difficult to collect (Choubin *et al.*, 2019). Moreover, avalanches formation is a complex process derived from the interaction between terrain, snowpack, and meteorological conditions. The release process of an avalanche is also heavily dependent on snow mechanics and snow properties, including snow texture. It is, therefore, not possible, at present, to predict a single avalanche event in time and space (Schweizer, Bruce Jamieson and Schneebeli, 2003).

Another approach for avalanche forecast and hazard mapping is based on the knowledge about the frequency and distribution of past snow avalanche activity (Muller *et al.*, 2021), which can be integrated with the current forecasting system. By knowing when and where avalanches have occurred in the past and by continuously monitoring avalanche activity in space and time, indicators are provided on snowpack stability and risk zones and periods can be better characterized (Giffard-Roisin *et al.*, 2020). All the data of the detected avalanches can then be merged to create an avalanche database consisting of time series of avalanche events with relevant information about location, size, time, type and much more. Despite its great value, this kind of data is scarce as its creation is limited by the terrain accessibility, the weather conditions and the danger of avalanches themselves (Sinha, 2019).

Recent advances in the mapping of avalanche events based on satellite data have great potential for creating such a database, as large areas can be continuously inspected even in inaccessible regions (Buhler, Hafner and Techel, 2021). Long-term avalanche monitoring over large regions can best be achieved using a spaceborne synthetic aperture radar (SAR) system, offering all-weather, day and night data, which ensures data continuity (Eckerstorfer *et al.*, 2019).

To detect avalanches from/in SAR data, target physical properties that can affect backscatter values, such as surface roughness and dielectric properties, are used (Kumar *et al.*, 2022). Changes in backscatter values between a reference SAR image and an activity SAR image can be used to distinguish between smooth and rough snow, making avalanche debris stand out.

Radar backscatter physics of snow

Radar (Radio Detection and Ranging) uses parts of the microwave band of the electromagnetic spectrum to measure the amount of energy backscattered by a target (Tedesco, 2015). SAR is a coherent radar system that uses the magnitude and phase of the received signals over successive pulses from elements of a synthetic aperture to create an image (European Space Agency, 2022a). The frequencies in which SAR operates are in the range 0.3-300 GHz (corresponding to wavelengths from 1mm to 1m), however the C-band frequency range is much smaller (4-8 GHz), which is ideal for penetrating tropical clouds and rain showers as it operates within an atmospheric transmission window (Lillesand, Kiefer and Chipman, 2015). The C-band does not penetrate vegetation canopies, thus it is restricted to the observation of top layers in areas with dense vegetation (European Space Agency, 2022b).

Backscatter is the portion of the radar signal that a ground feature redirects directly back towards the radar antenna, and it is expressed as a ratio between the scattered power and incident power at ground level (Small, 2011). The scattering cross-section in the direction toward the radar is called the backscattering cross section, and its usual notation is the symbol sigma (σ). Sigma is the conventional measure of the strength of a radar signal reflected from an object. Sigma nought (σ0) represents the scattering coefficient, which is the normalized dimensionless estimation of the backscatter per given reference area, namely the size of one single pixel (Dostalova *et al.*, 2022). The backscatter coefficient sigma nought can also be represented as beta-nought (β0) or gamma-nought (γ0). *Beta nought (β0),* the radar brightness, is the basic calibration of a SAR product that makes use of an internal calibration constant stored in the metadata. *Sigma nought (σ0)* is the normalized radar cross-section, an advanced measure of calibration that considers the calibration constant and the incidence angle. *Gamma nought (γ0)* makes additional use of the local incidence angle for geometric correction. Usually, Gamma nought is used to compare backscatter values of SAR images obtained from different angles. If SAR data from the same orbit and path is used, sigma nought is the preferred measure to identify backscatter changes between two images.

A specific model that applies to backscatter proprieties of snow avalanches is currently not available (Eckerstorfer and Malnes, 2015); however, following general scattering physics from bi-continuous media and rough surfaces, scattering in snow increases with the increasing length of ice grains (Wiesmann, Mätzler and Weise, 1998), with increased surface roughness and with decreasing incidence angle (Leinss *et al.*, 2020). This allows the location of the rough snow resulting from avalanche debris by searching for areas with higher backscatter values.

Avalanche mapping using remote sensing

Remote sensing of avalanches is a recent and fast-developing scientific field (Wesselink *et al.*, 2017) that was introduced with the application of hazard mapping using multitemporal SAR images for avalanche detection. At its early stage, it was mainly based on expert interpretation (Wiesmann *et al.*, 2001). More recently, classification and segmentation algorithms were developed to automatically identify avalanches, e.g., Wesselink *et al*., (2017) used an automatic detection algorithm based on backscatter thresholding, but the method has the drawback of marked over-detection. Vickers et al., (2017) used change detection and K-means classification and applied improved filtering on the images to obtain satisfactory detection results. Eckerstorfer *et al*., (2019) used a near-real-time detection system that achieves an accuracy of 79% in cases of medium to large avalanches, which is already operational in some regions of Norway.

A different approach consists of a colour-based detection method applied to SAR image time series, that detects, at best, 70% of verified avalanches (Karas *et al.*, 2022). Recent work has also focused on avalanche detection in SAR images by applying deep learning methods, e.g., Sinha *et al*., (2019) used convolutional neural networks (CNN) to locate avalanche debris signatures on SAR image patches. Bianchi *et al*., (2021) applied the same method but approached the segmentation task at the pixel level instead of the patch level, making the segmentation independent of the window size. The mentioned methods are very promising; however, they rely on expert labelling, which brings along limitations, e.g., reliability, availability of an expert able to train large datasets, and difficulties in differentiating between new avalanches and (still visible) old ones. Sinha *et al*., (2019) proposed deep unsupervised learning using a variational autoencoder (VAE) as a new benchmark in avalanche detection that outperforms previous methods. Although labelled data is only required in the validation phase, a form of training by an expert is still required.

Successful attempts have also been made to detect avalanches using optical imagery instead of radar. Bühler et al. (2019) used very high-resolution Spot 6/7 data to manually delineate avalanches obtaining high accuracy. Hafner et al. (2022), using the same type of data, applied a state-of-the-art deep learning model to identify avalanches automatically. The limitation of optical data is the availability of high-resolution images, which can be costly. Freely available data can be obtained from the Sentinel-2 imaging mission that samples 13 spectral bands using the MultiSpectral Instument (MSI) with a five-day revisit frequency. Four bands have a spatial resolution of 10 meters, while the others have 20- or 60-meter resolution. Sentinel-2 data has been tested for the detection of avalanches, however, its resolution has been deemed too coarse for meaningful avalanche mapping (Buhler, Hafner and Techel, 2021). Hafner *et al*., (2021) attempted an evaluation of performance and completeness by comparing optical and radar imagery and confirmed the reliability of Sentinel-1 SAR data for avalanche detection.

Problem definition

Avalanche prevention end research is usually performed on a regional scale by local authorities or independent research institutes. In some cases interregional and international collaborations are put in place, e.g., the newly created unified avalanche forecast bulletin that covers the previously mentioned regions of Trentino and Alto Adige in Italy, and the region of Tyrol in Austria (Euregio, 2022).

In the Trentino-Alto Adige region (Trentino-Süd Tirol) avalanches are mapped only in cases they cause injuries to people or damage to infrastructure. Data from these mapped avalanches is stored and managed by the local authorities and is publicly available through an online GIS platform. Avalanches that do not cause injuries or damage are sometimes registered if they are reported by eyewitnesses that happen to see the event and are willing to inform the authorities. However, these reports do not always contain exact information about location, size, release date, and time, and are thus not included in the official avalanche database. Hence, it can be estimated that only a fraction of all avalanches is recorded and mapped. Local authorities in this region, responsible for avalanche prevention and forecast, have no data at their disposal regarding released avalanches other than the aforementioned mapped events, as attempts to create a regional database containing all the detected avalanches have not been made yet. This knowledge was gained through the author's direct questioning to regional avalanche prevention offices.

The creation of a regional avalanche database is possible if a reliable, fast, and easy-to-use model is available that can identify avalanches from satellite imagery with broad coverage and ensure data continuity. A constellation of freely available Sentinel-1 SAR (A&B) data can be used to reduce temporal resolution from twelve to six days. This applies only until December 2021, after which SAR data from the Sentinel-1 B satellite is unavailable due to an uncertifiable malfunction of the power unit that forced the mission to end. A replacement satellite in programmed but has not been launched yet (ESA, 2022).

Once SAR data is downloaded, the detection of avalanches can be performed by applying change detection. Such detection can be either manual, semi-automatic or automatic. Manual avalanche identification relies on the expert interpretation that is subject to observer bias and challenging to reproduce. On the other hand, (semi-)automatic mapping methods can ensure reproducibility and transferability of the methods to some extent but needs further investigation.

Aims and objectives

This study aims to create a model to semi-automatically identify occurred avalanches within the western part of the Trentino-Alto Adige region using Sentinel-1 (C-band) SAR data utilizing unsupervised object-based classification. The efficacy of the model is then tested by comparing the results to reference data from officially registered avalanches to assess the accuracy and reliability of the SAR semi-automatically detected avalanches. The freely available Sentinel-1-SAR data from European Space Agency (ESA) Copernicus were used, with the Ground Range Detected (GRD) Interferometric Wide swath (IW), and dual-polarisation mode images in vertical-vertical (VV) and vertical-horizontal (VH) polarisation. Both Sentinel-1 SAR A&B satellites were used to reduce the temporal baseline to six days; the ascending flight direction (south-north) was chosen for analysis since complete coverage of the investigation area is guaranteed always using the same orbital path (117) and frame (148) for both Sentinel-1 A&B satellites.

The main objective of this research is to utilize SAR data to detect avalanche debris, by identifying changes in the SAR backscatter intensities caused by the rough snow surface created by the debris deposited in the avalanche's runout zone. Detection is performed by creating and comparing image pairs consisting of an active Sentinel-1 SAR image (where avalanches are potentially present) with a reference Sentinel-1 SAR image taken six days previously, applying change detection technique and unsupervised object-based classification. Further objectives are assessing the accuracy of SAR avalanche detection, comparing results with mapped avalanches, and comparing the correct detection rate of VV- and VH-polarised data. The following research questions were defined: can SAR data be applied to detect avalanche debris in the investigation area, and with what accuracy? Which avalanche size can best be detected? Which SAR polarization returns best results?

Materials / Methods

In this chapter the selected investigation area is introduced, the data employed for analysis is presented in more detail, and finally the workflow utilized to detect and validate avalanche debris using Sentinel-1 SAR data is exposed.

Investigation Area

The investigation area consists of the western part of the Trentino-Alto Adige region in northern Italy. (Figure 1). The area covers approximately **3,640** km^2 and consists of inhabited alpine valleys designated for fruit tree cultivation, vineyards and pastures surrounded by peaks reaching 3900 meters above sea level. The area was chosen mainly for three reasons: the familiarity of the author with its geography; data availability with regards to officially mapped avalanches by local authorities, used as reference data; and the fact that avalanche detection from SAR data has not yet been tested here, and results could be very much needed by local authorities that possess very little information about past avalanche events. The region is divided into two provinces, **Trentino,** and **Alto Adige** (hereinafter "South Tyrol") that operate independently on an administrative level. For this reason, all data other than SAR images was obtained from two different sources and therefore needed to be integrated. Due to this divergence in data sources, in some cases analysis was performed differently for each region, which produced diverging results. I will be often referring to the two different investigation areas, namely the region of Trentino as opposed to the region of South Tyrol.

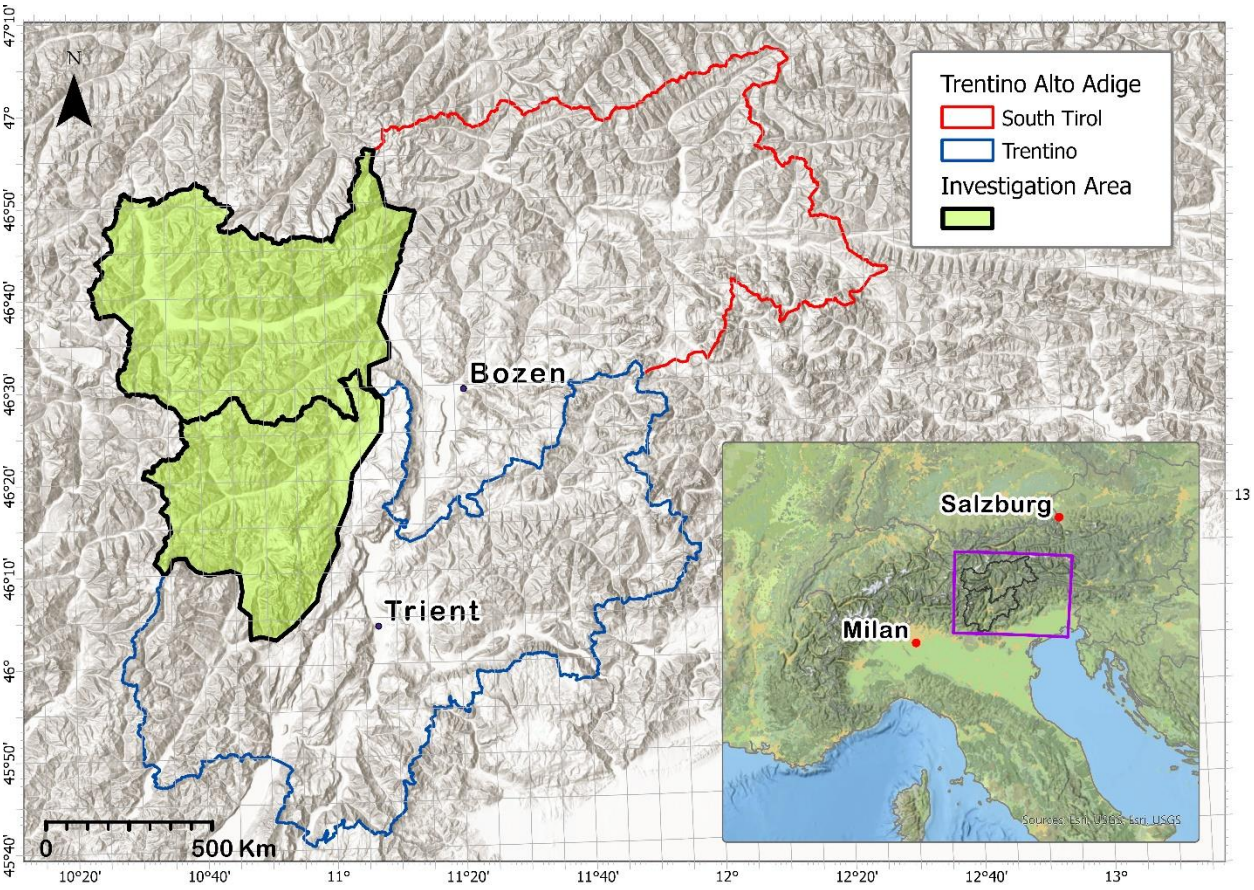

Figure 1: The Trentino-Alto Adige region of interest with the investigation area highlighted in green.

Data

The required data for this research consisted of the **Sentinel-1 SAR images**, **mapped avalanches**, a **digital elevation model (DEM)**, various types of **land cover** polygons and general **meteorological** information for selected periods. The data is described in more detail in the next three sections. The reference period chosen was the winter season 2017-2018, which was marked by a particularly high avalanche activity record. I decided to obtain SAR data starting from 01/11/2017 to 01/05/2018. All data was either directly acquired in, or reprojected into the coordinate reference system WGS 1984, UTM Zone 32N. SAR data was downloaded from the Alaska Space Facility's (ASF) DAAC (ASF, 2022); meteorological data was obtained from the official weather departments of each region, i.e. Meteotrentino for the Trentino region (Meteotrentino, 2022), and Süd Tirol Wetter for South Tyrol (Weather South Tyrol, 2022a). All other data was downloaded from two web GIS platforms: "WebGIS" for the Trentino Region (Provincia Autonoma di Trento, 2023) and "GeoKatalog" for the South Tyrol (Suedtiroler Buergernetz, 2023).

Sentinel-1 SAR data

Remote sensing of avalanches can be implemented using optical, LiDAR and radar sensors. While terrestrial LiDAR is the best choice for small scale monitoring (e.g., ski resorts), for the regional scale, optical- and radar satellite data is more suitable. Optical data excels in the detection of the complete avalanche (from start to depositional zones). However, its acquisition is hindered by weather, shaded areas and darkness (Eckerstorfer *et al.*, 2016). Furthermore, high- and very high-resolution optical satellite data is not freely available. For the mentioned reasons, this research was built around Sentinel-1 SAR data which is freely available, covers large areas and is weather-and light-independent.

Sentinel-1 mission from the European Space Agency (ESA) consist of a constellation of two satellites, Sentinel-1A that was launched on 03/04/2014 and Sentinel-1B that was launched on 25.04.2016. Each Sentinel satellite rotates in a near-polar, sun-synchronous orbit with a 12-day repeat cycle; however, when using both satellites the revisit time can be reduced to six days. Sentinel-1 operates in the C-band, which refers to the wavelength of microwaves produced by the SAR antenna that influence the amount of ground penetration that occurs. C-band has a wavelength of approximately 6 cm, which works well in the analysis of snow and ice (Flores *et al.*, 2019).
Currently, the Sentinel-1B satellite is out of order due to a technical malfunction occurred in December 2022, thus data availability is currently limited to a revisit time of 12 days. ESA is planning to launch Sentinel-1C as replacement as soon as possible (ESA). However, this does not affect what presented here.

For this research, the Interferometric Wide swath (IW) data acquisition mode is used, and High Resolution (HR) Ground Range Detected (GRD) products are downloaded. IW is Sentinel-1's primary operational mode over land and acquires data in three swaths using the Terrain Observation with Progressive Scanning SAR (TOPSAR) imaging technique, with a total swath width of 250 km. GRD is Level-1 processed, focused SAR data that has been detected, multi-looked and projected to ground range with a spatial resolution of 20 m and 10 m pixel spacing. The system records in a dual-polarisation mode so that images in vertical-vertical (VV) and vertical-horizontal (VH) polarisation are available; both are analysed and compared. Theoretically, cross polarisation is more sensitive to surface roughness, therefore a higher degree of detected avalanche debris is expected in VH mode (Wesselink *et al.*, 2017). The ascending orbit was chosen for analysis since complete coverage of the investigation area is guaranteed using the same orbital path (117) and frame (148) from both satellites.

For the reference period, 29 SAR images were downloaded starting from 02/11/2017 and ending on 25/04/2018 (Table 1). The image from 31/01/2018 was not available and could not be included in the analysis. In that case an image pair was created with a reference image

(Nr 15) originating 12 days before the activity image (Nr.16). When referring to specific SAR scenes, the date of acquisition will be used to identify data.

Table 1: All queried Sentinel-1 SAR scenes from Sentinel-1 A&B satellites (S1A, S1B), Interferometric Wide (IW) acquisition mode, Ground Range Detected High Resolution (GRDH) products.

Nr.	SAR data (file names)	Acquisition Date
1	S1A_IW_GRDH_1SDV_20171102T170650_20171102T170715_019089_0204A4_**4D2C**	02/11/2017
2	S1B_IW_GRDH_1SDV_20171108T170607_20171108T170632_008193_00E7AB_**483F**	08/11/2017
3	S1A_IW_GRDH_1SDV_20171114T170650_20171114T170715_019264_020A1A_**F4ED**	14/11/2017
4	S1B_IW_GRDH_1SDV_20171120T170607_20171120T170632_008368_00ED01_**6542**	20/11/2017
5	S1A_IW_GRDH_1SDV_20171126T170650_20171126T170715_019439_020FA4_**80C2**	26/11/2017
6	S1B_IW_GRDH_1SDV_20171202T170606_20171202T170631_008543_00F27E_**F5CB**	02/12/2017
7	S1A_IW_GRDH_1SDV_20171208T170649_20171208T170714_019614_021517_**5766**	08/12/2017
8	S1B_IW_GRDH_1SDV_20171214T170606_20171214T170631_008718_00F80B_**318F**	14/12/2017
9	S1A_IW_GRDH_1SDV_20171220T170649_20171220T170714_019789_021A8B_**3F0E**	20/12/2017
10	S1B_IW_GRDH_1SDV_20171226T170605_20171226T170630_008893_00FDA5_**6D94**	26/12/2017
11	S1A_IW_GRDH_1SDV_20180101T170648_20180101T170713_019964_021FFD_**DA78**	01/01/2018
12	S1B_IW_GRDH_1SDV_20180107T170605_20180107T170630_009068_010357_**6D1E**	07/01/2018
13	S1A_IW_GRDH_1SDV_20180113T170648_20180113T170713_020139_022586_**37C5**	13/01/2018
14	S1B_IW_GRDH_1SDV_20180119T170604_20180119T170629_009243_010909_**C1F9**	19/01/2018
15	S1A_IW_GRDH_1SDV_20180125T170647_20180125T170712_020314_022B12_**55C4**	25/01/2018
16	S1A_IW_GRDH_1SDV_20180206T170647_20180206T170712_020489_0230A8_**CEBB**	06/02/2018
17	S1B_IW_GRDH_1SDV_20180212T170604_20180212T170629_009593_011490_**1254**	12/02/2018
18	S1A_IW_GRDH_1SDV_20180218T170647_20180218T170712_020664_02363D_**7BD**	18/02/2018
19	S1B_IW_GRDH_1SDV_20180224T170604_20180224T170629_009768_011A52_**F6C8**	24/02/2018
20	S1A_IW_GRDH_1SDV_20180302T170647_20180302T170712_020839_023BC9_**95C6**	02/03/2018
21	S1B_IW_GRDH_1SDV_20180308T170604_20180308T170629_009943_01202F_**95AD**	08/03/2018
22	S1A_IW_GRDH_1SDV_20180314T170647_20180314T170712_021014_024156_**7412**	14/03/2018
23	S1B_IW_GRDH_1SDV_20180320T170604_20180320T170629_010118_0125E3_**8ACB**	20/03/2018
24	S1A_IW_GRDH_1SDV_20180326T170647_20180326T170712_021189_0246E6_**43BC**	26/03/2018
25	S1B_IW_GRDH_1SDV_20180401T170604_20180401T170629_010293_012B8E_**B148**	01/04/2018
26	S1A_IW_GRDH_1SDV_20180407T170647_20180407T170712_021364_024C61_**AD8B**	07/04/2018
27	S1B_IW_GRDH_1SDV_20180413T170605_20180413T170630_010468_01313A_**F3C6**	13/04/2018
28	S1A_IW_GRDH_1SDV_20180419T170648_20180419T170713_021539_0251D6_**261E**	19/04/2018
29	S1B_IW_GRDH_1SDV_20180425T170605_20180425T170630_010643_0136C7_**4F22**	25/04/2018

SAR data is used to detect the debris zone of an avalanche, which refers to the snow that accumulates in the bottom section where the avalanche stops. This area is also called **zone of deposition** (Figure 2), as opposed to the transition zone that is the central part of the avalanche and the most upslope area, the release zone, characterized by a smooth surface caused by the failure of the weak layer (Leinss *et al.*, 2020). The deposition zone consists of densely compacted snow granules which create a change in snow depth and density, as well

as surface roughness (Muller *et al.*, 2021). Both the rough surface and the debris volume scatter radiation more omnidirectionally (diffuse scattering) compared to an undisturbed snowpack over smooth ground (specular scattering). Diffuse scattering leads to more radiation returning to the SAR antenna and thus to higher values in backscatter. It is the deposition zone of an avalanche that causes the change in backscatter values that can be observed in SAR data.

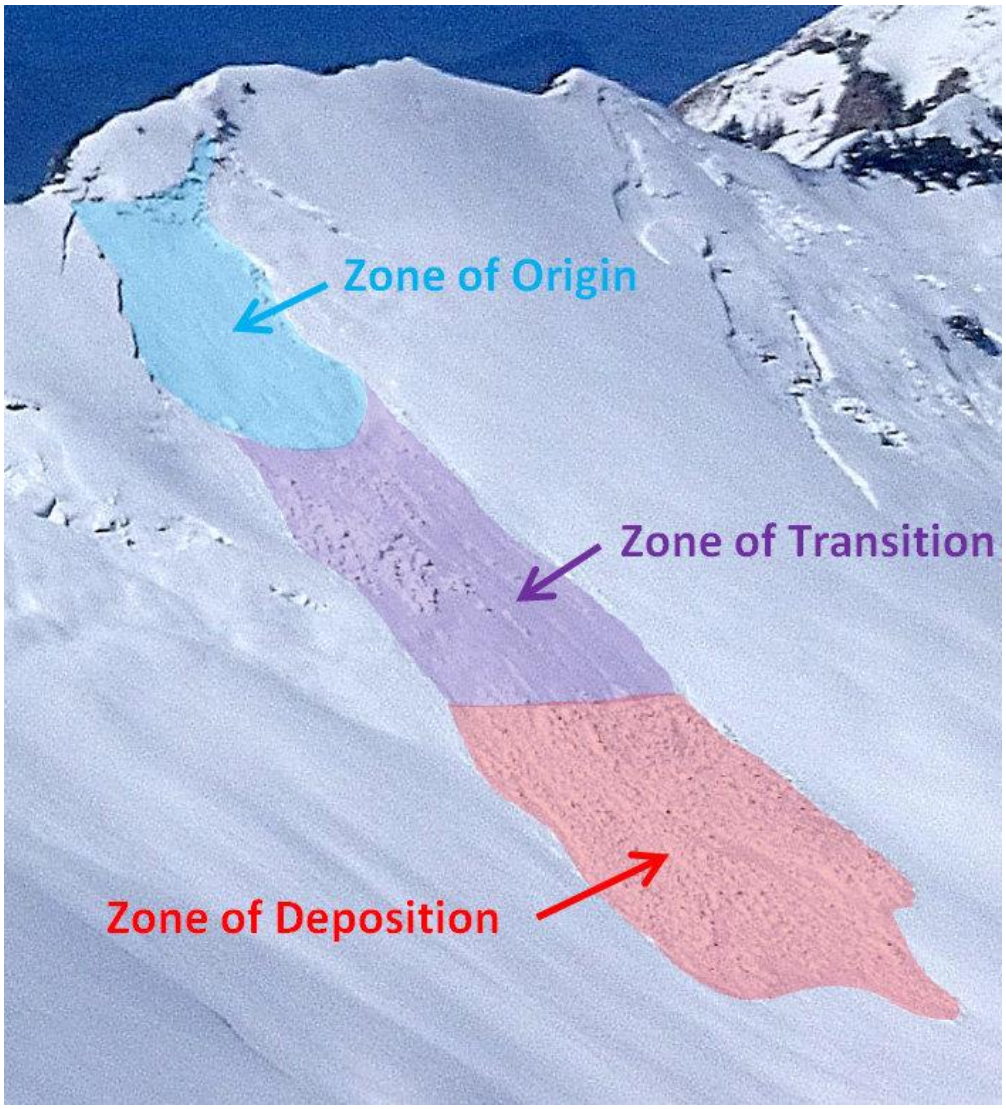

Figure 2: Snow avalanche taken as example to show the subdivision into zone of origin, where the avalanche is triggered; zone of transition and zone of deposition where snow runs out and produces a rough surface (Figure adopted from Leinss et al. 2020).

Layover and Shadow

SAR data is subject to geometry distortions that cause, among other effects, relief displacement. These effects are caused by the side looking system of radar antennas. When a vertical terrain feature is encountered by a radar pulse, the top of the feature is hit before the base and the return signal from the top will get back to the antenna before the return signal from the base. This effect is called layover and causes e.g., the top of the mountain to lean toward the nadir and hide areas lying underneath. Another relief displacement effect is the radar shadow, where slopes facing away from the radar antenna will return weak signal or no signal (Lillesand, Kiefer and Chipman, 2015). In a mountainous research regions radar shadow and layover can affect a large amount of the terrain, sometimes up to 50% of it (Wesselink *et al.*, 2017). Shadow and layover areas must thus be exempted from the analysis because they do not contain valuable information and could lead to wrong interpretation. Using Sentinels Applications Platform (SNAP) software it is possible to create a layer that contains pixel with values greater than 0 identifying shadow or layover areas. This mask layer is then exported in form of an additional band making it possible to visualize the layer in any GIS software.

Mapped avalanches

Data of officially registered and mapped avalanches was used as reference to verify the reliability of the semi-automatically detected events. This data was obtained from two different sources based on the location of the avalanches.

In the Trentino region 5,736 avalanches have been mapped since 1985. Taking only the investigation area into consideration, 1,710 events have been mapped since record began. This dataset has the major drawback that the dates of single avalanches are not contained within the data. Dates, when available, must be extracted manually by accessing a pdf documentation file attached to every single event. This task, however, could not be accomplished within the framework of the present research.

In the South Tyrol region 1165 avalanches have been mapped starting with the winter season 2007-2008, of which 96 fall within the boundaries of the investigation area. Considering only the reference winter season, 49 avalanches are available as ground truth. Mapped avalanches are accompanied by information about name, size and, more importantly, release date. This data was used as reference data to validate avalanches semi-automatically detected by the proposed model. Mapped avalanches for both investigation regions are shown in Figure 3.

Not all mapped avalanches could be used as reference data for some lay within the masked-out areas. Table 2 gives an overview of how many mapped avalanches were available to be compared to the semi-automatically detected ones. The table shows the number of total

mapped avalanches and the number of avalanches that lie within areas were SAR avalanche detection is hindered by topological factors or by radar and shadow layover. Mapped avalanches were counted as "not detectable" by SAR when they lay completely within one of the masked-out locations. All mapped avalanches were counted and only in the last row was the count restricted to the winter season 2017-2018.

Table 2: Mapped avalanches availability divided for the two regions of interest.

	South Tyrol	**Trentino**
Total of mapped avalanches	221	855
Within forest	6	109
Within radar shadow or layover	5	109
Within water bodies	0	0
All SAR detectable avalanches	210	653
SAR detectable avalanches season 2017/2018	**49**	No data available

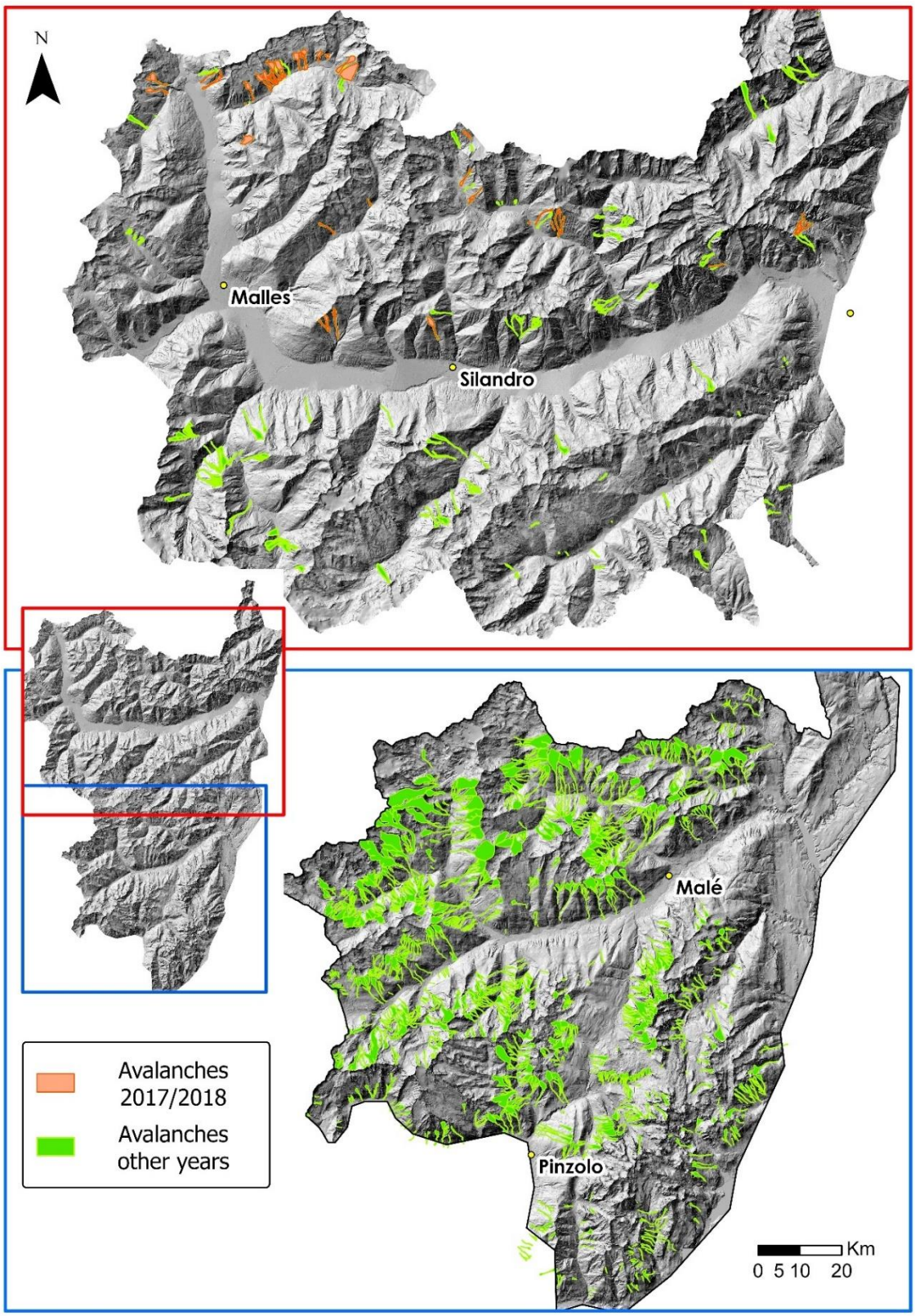

Figure 3: Mapped avalanches available as reference data for the South Tyrol region (above) and the Trentino (below) region. In Trentino avalanches have no specification about the event date, accordingly they fall into the category "avalanches other years".

Manually detected avalanches

Table 2 shows that the final number of mapped avalanches available to be used as reference data to verify the semi-automatically detected avalanches is limited. The problem derives from the location of detected avalanches that often corresponds to areas where SAR backscatter derives from terrain features different than snow. In fact, it is often avalanches that reach lower altitudes and obstruct roads or damage buildings that are witnessed, reported, and consequently mapped. These events often happen to be in forested areas or close to urban settlements, areas which were masked out form investigation. To overcome this shortage of reference data, manual avalanche identification based on expert interpretation of RGB image composites was applied to create an additional validation data set to be integrated with the available mapped avalanches. The process of manual avalanche mapping will be presented in more detail in the results section.

Miscellaneous data

DEM

A Digital Elevation Model (DEM) was used for the creation of two separate masks. The DEM was created from two separate DEM's, one for each region. The first DEM covering the South Tyrol region had a resolution of 2.5 meters and was resampled to 5 meters. The second DEM for the Trentino region was derived from LiDAR data with a resolution of 1 meter and was also resampled to 5 meters. The datasets were then seamlessly merged.

Land cover

Land cover data was acquired for both regions in order to screen out areas where avalanches cannot occur or areas where SAR signals can be disturbed by features other than snow cover. Those areas include forested areas, water bodies and urban settlements. More information about the reasons why these areas are unsuitable for SAR avalanche detection can be found in the workflow chapter.

Some literature suggests to mask-out glaciers and agricultural surfaces from the analysis due to their sensitivity to snow cover changes (Eckerstorfer *et al.*, 2019). I decided not to mask-out glaciers since they cover large areas of the alpine zone (over the tree line) and valuable information about avalanche activity can be found in these areas. Glaciated surfaces show high sensitivity to snow cover change especially in the early part of winter when the first snow starts to fall (Eckerstorfer *et al.*, 2019). Agricultural surfaces extending to the foothills of mountains are highly common especially in the Vinschgau valley (South Tyrol) and its side valleys. Therefore, agricultural surfaces were kept in the analysis area because avalanche debris is likely to be deposited there. Special attention was given to the analysis of early winter images (November and December) with regards to avalanche activity registered over glaciers, and to the analysis of avalanche deposit detected over agricultural areas.

Meteorological data

Meteorological data was used to pinpoint time periods or specific days were avalanche activity was more likely. Avalanches are expected when triggering factors are present. Artificial triggering factors (e.g., loading effect caused by a skier) cannot be determined for past avalanche events. However, natural triggering or spontaneous release situations caused by precipitation or temperature rise can be inferred analysing meteorological data. One meteorological station was chosen as reference for each investigation region. Even though data from only one station cannot represent the exact meteorological events of the whole region, the information was sufficient to get a general picture of precipitation values (snow and rain) and the general temperature curve so that days with exceptional events could be picked out. Meteorological data contained in Table 3 shows chosen days with major snowfall for the selected meteorological stations taken as reference for Trentino (station of Folgarida), and South Tyrol (station of Schlanders).

Table 3: amount of fresh snow registered at two selected meteorological stations for the two regions of interest. Only days with a considerable amount of precipitation were chosen and displayed.

Schlanders (South Tyrol)		**Folgarida (Trentino)**	
Data	**New snow (cm)**	**Date**	**New snow (cm)**
05/01/2018	21,1	11/12/2017	26
09/01/2018	21,6	12/12/2017	41
21/01/2018	18,5	28/12/2017	53
22/01/2018	11	02/02/2018	28
08/03/2018	4,7	12/03/2018	19
12-13/04/2018	15,8	16/03/2018	18
16/04/2018	6,6	30-31/03/2018	20

Workflow

An overview of the general workflow is described first and represented in form of a graphic (Figure 4), whereas a detailed presentation of each single step will be given in the following sections.
Downloaded SAR data needed to undergo several pre-processing steps before analysis. Once ready, SAR image pairs were created to perform change detection. Areas where avalanches are not expected were excluded from analysis. Image pairs consisted of a reference image (used as baseline) and an activity image originated six days later (where avalanches could potentially be present) and were used to create a change detection image subtracting the reference image form the activity image. A median filter was applied to reduce noise but preserve edges (Leinss et al., 2020). For each reference-activity image pair, two change detection images are created, one in co-polarisation VV and one in cross-polarisation VH. In the next step, iterative self-organizing (ISO) and K-means data analysis techniques were tested to produce classes consisting of pixel clusters with similar reflection values. This task was performed using both ArcGIS Pro and the semi-automatic classification plugin (SCP) in QGIS (Congedo, 2023). The resulting classes were analysed and subdivided into avalanche and non-avalanche. All analysis steps except pre-processing and the k-means semi-automatic classification were performed using ArcGIS Pro.

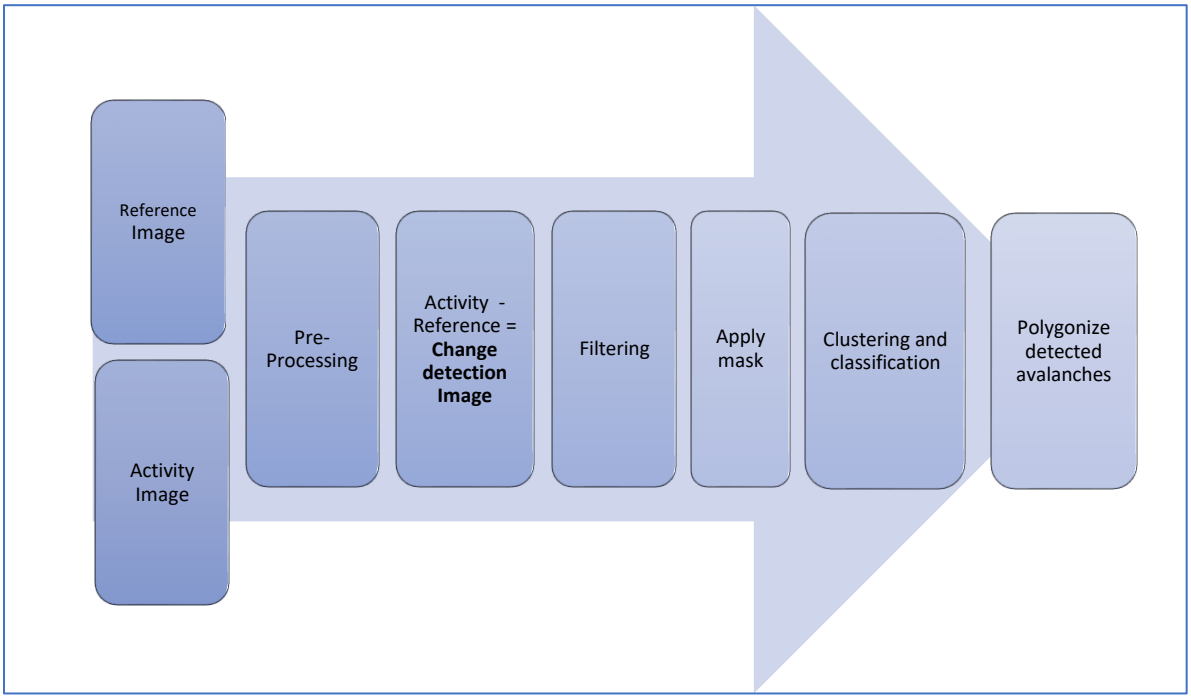

Figure 4: General workflow employed to process Sentinel-1 SAR data to obtain clusters of possible avalanche debris.

Pre-processing

Sentinel-1 SAR GRD products are Level-1 focused data that has been pre-processed by the Instrument Processing Facility (IPF) via the application of various algorithms including pre-processing, Doppler centroid estimation, single look complex focusing, and image and post-processing. GRD products are projected to ground range using the Earth ellipsoid model WGS84; they contain the detected amplitude and are multi-looked to reduce the impact of speckle (European Space Agency, 2022b). Using ESA's SNAP software, further pre-processing steps are applied before analysis is performed. Certain steps require a digital elevation model to perform terrain corrections; in these cases, an external DEM was chosen with a resolution of 5 meters.

The procedural steps employed are as follows:

1. Create subset: From the whole SAR dataset I select a smaller subregion containing only the investigation area to speed up processing that can be quite slow especially in the terrain flattening step.
2. Apply orbit file: SANP automatically downloads the appropriate orbit file from ESA archive and applies it to the image. The file contains accurate information about the satellite's position and velocity and is used to update inaccurate orbit state vectors contained within the metadata information of SAR products (Filipponi, 2019).
3. Calibrate data: Calibration consist in converting digital pixel values to radiometrically calibrated SAR backscatter, represented by sigma nought values. The sigma nought varies depending on the incidence angle, wavelength, and polarisation, as well as with properties of the scattering surface (Filipponi, 2019). I create an output for sigma nought, gamma nought and beta nought.
4. Flatten terrain radiometrically (RTF): Rugged terrain can induce variations in radar backscatter values. RTF is a method that minimizes these variations with the support of a DEM (Dostalova et al., 2022).
5. SAR simulation: A mask is created containing all areas of shadow and layover. This step was performed only once on a selected image as all images have the same geometry and thus the same shadow and layover areas.
6. Range-Doppler Terrain Correction (own DEM + CRS). In SAR data, geometric distortions induced by side-looking imaging and rugged terrain can cause pixels to be displaced and thus terrain to be distorted. Terrain correction compensates for these distortions. Range Doppler terrain corrections uses a digital elevation model to correct the location of each pixel (Filipponi, 2019). The target Coordinate Reference System (CRS) was selected and set to match the UTM zone based on the geographic location of the image.

The speckle filtering process was not performed since it might have removed small spatial structures, the detection of which is required for the identification of avalanche debris (Filipponi, 2019). After pre-processing is performed, the image is exported for further analysis. The image contains four bands: sigma nought cross- and co-polarisation, and gamma nought cross- and co-polarisation.

From power to Decibels (dB)

The standard output of the Radiometrically Terrain-corrected (RTC) process is a gamma nought power image, to which the optional sigma nought power image was added. Those formats, when displayed in a GIS software, appear dark, making them difficult to use for visual analysis. Therefore, for a better visualisation and for analysis, the unitless backscatter coefficient is converted to decibels (dB) using a logarithmic transformation "SAR Image dB" = 10 * Log10 ("SAR image") (Alaska Satellite Facility, 2022). In order to apply this calculation to both polarisation bands VV and VH of both the reference and activity image, a processing model is built to improve efficiency. The model includes a clipping procedure, where the SAR data is cut to the shape of the investigation area.

Masks

Object based classification performed to identify snow accumulation derived from avalanches often produces false alarms, i.e. areas of increased backscatter in the radar signal caused by factors different from avalanche debris (Bühler *et al.*, 2018). To reduce false avalanche detections and the missing of smaller to medium size avalanches, three masks were created and tested to confine locations where avalanche debris can realistically be found and areas where it can be excluded. The layover and shadow mask mentioned in the previous chapter needs to be added, which brings the total number of applied masks to four (Figure 5).

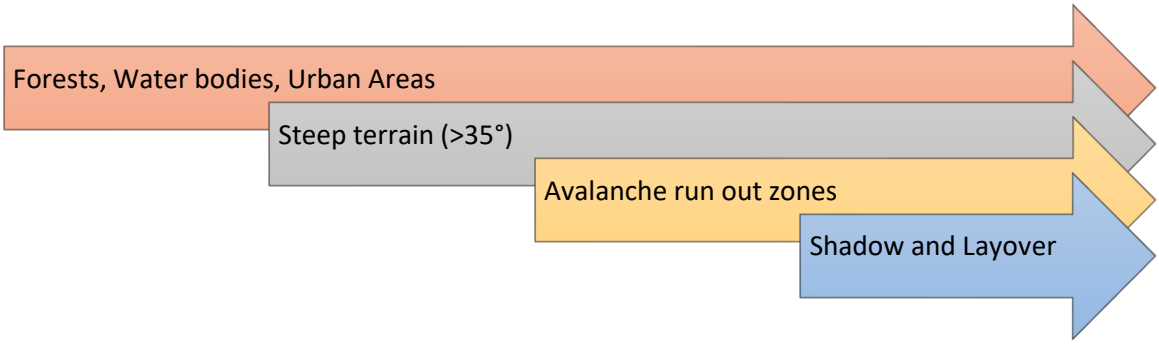

Figure 5: The four layers of masked-out areas for which analysis was not performed due to the unlikelihood of avalanche debris to be deposited.

The *first* mask consisted of forested areas, water bodies and urban areas, which were masked-out from the investigation area. As C-band radar does not penetrate forest as the return signal originates from the treetops and not from ground features where avalanche deposit may be found. Avalanches, in general, tend to be blocked by dense vegetation acting as a natural barrier against snow; however, there are exceptions to that, especially when it comes to wet snow avalanches. Avalanches detection was not performed for urban areas since only exceptional events reach villages or towns, and SAR signals may be disturbed by artificial features such as buildings or roads. Finally, water bodies were also excluded because it is uncommon for an avalanche to be deposited on a completely flat surface like a lake, and if that happens the lake must be frozen for debris to remain on the surface. Rivers are ignored in the analysis because in the investigation area they typically fall outside avalanche runout zones. Whereas streams, found on steeper terrain in the mountains, can be completely covered by snow in winter so that avalanches could potentially be detected there. The second mask, derived from the DEM, was based on slope. If a slope is too steep debris cannot accumulate, in fact it is unlikely to be found, except for very small avalanches, on terrain steeper than 35° (Bühler et al., 2009). Areas steeper than that were masked out from the investigation area. The *third* mask is based on **avalanche runout zones**, which refers to the area where debris is likely to be found. There are two approaches for defining runout

zones: using the toolbox named "Terrain Analysis Using Digital Elevation Models" (TauDEM) (Tarboton, 2023), or evaluation based on slope. The simpler approach based on slope implies that avalanche debris can only be found on terrain with a certain steepness. Here opinions differ, e.g., Wesselink et al. locate this range between 5° and 55°; Vickers et al. use 0°- 40° and Bianchi et al. state that avalanche debris pixels are usually found between 20° and 35° steepness. The more advanced method infers the runout zone based on the Potential Release Area (PRA) of an avalanche using the TauDEM toolbox, which is composed of tools for extracting and analysing hydrologic information from topography and has a specialised function that evaluates potential avalanches runout zones. PRA is determined using a python script (Bertschinger, 2022), based on Bühler et al., (2018) that calculates areas where avalanches are likely to be triggered based on four input parameters: minimum and maximum slope, maximum curvature and minimum polygon area.
The best parameter configuration, chosen after Bühler et al. (2013), together with a description of the parameters' action, is shown in Table 4.
The output is a raster with cell values of 1 for PRA areas, and cell values of 2 for no PRA areas. This raster was then transformed into a polygon feature class and reclassified so that PRA polygons were assigned the value 1, and non-PRA polygons were assigned the value 0.

Table 4: Description and chosen values of the parameter that can be fine tuned before executing the Potential Release Area (PRA) algorithm.

Parameter	Description	Chosen value
Minimum slope	The minimum slope angle required for a mass of snow to start sliding downhill	30°
Maximum slope	The maximum slope angle beyond which avalanches usually do not trigger since snow does not accumulate if a slope is too steep	60°
Maximum curvature	Maximum terrain curvature beyond which it is assumed that an avalanche cannot be triggered	6
Minimum area	Polygons smaller than this threshold will be merged with larger neighbouring polygons. This is required for the simplification process	2000 m

In the next step the TauDEM Toolbox was used to infer the runout zones. Three separate steps are needed to obtain the result:

1. From the DEM, grid cells surrounded by higher terrain are filled using a flooding algorithm so that sinks are eliminated, and a drainage path can be determined from each grid cell (Pit Filled Elevation Grid)
2. A flow direction is assigned to each cell based on steepest slope recorded as an angle in radians anticlockwise from east, based on the algorithm described by Tarboton (Tarboton, 1997) (D-infinity Flow Direction Grid).
3. The avalanche runout is calculated using the outputs of step 1 and 2 as inputs, together with the previously created PRA, comprised of positive values where avalanches may be triggered and zero values elsewhere (D-Infinity Avalanche Runout). The avalanche runout identifies area affected by avalanche debris and also the flow path length to each cell in the affected area (Tarboton, 2023). Two parameters can be fine tuned: the maximum slope angle between the source cell and the affected area, below which a cell is not identified as runout area; the second parameter is the threshold (0.2) that controls the excess downslope dispersion of flow cells created by step 2, which are cells that sometimes lead to an overestimation of the affected flow area.

The result of the three processing steps performed with the TauDEM toolbox is a raster with values ranging from 20 to 90 which refer to the angle (in degrees) from the cell to its source site. Higher values represent a runout zone resulting form steeper terrain above, which makes it more likely for an avalanche to stop there.

This research aims at detecting avalanche debris within the boundaries of avalanche runout zones; therefore, a simplified binary map was created that partitions the investigation area into zones where runout is possible, and zones where runout is not expected (Figure 6).

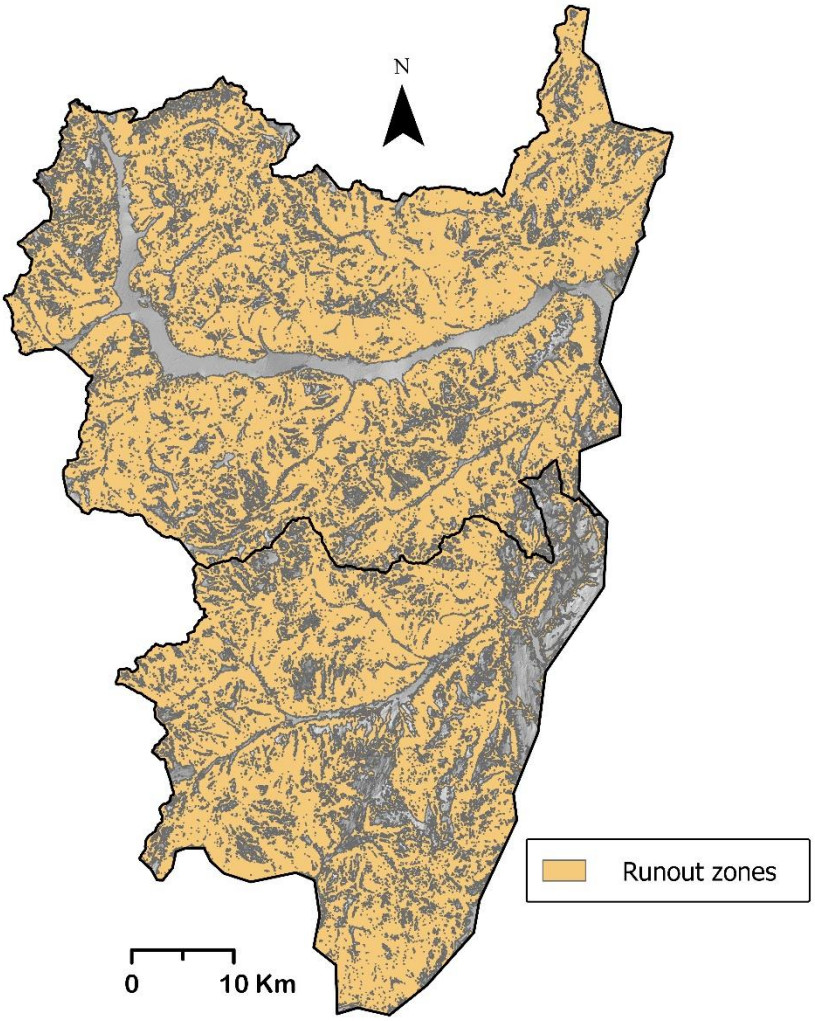

Figure 6: Binary map that partitions the investigation area into zones of possible runout, and zones where runout is not expected.

Manual avalanche detection

In the manual avalanche detection process, referred to as RGB differentiation, a composite image is constructed where the red and blue channels contain the reference image, and the green channel contains the avalanche activity image. This allows pixels that show increased backscatter values between the reference and activity image to appear green, pixels with decrease in backscatter appear purple and pixel that witnessed no change appear grey. Usually, avalanche debris resemble elongated, tongue-shaped and downslope-extending features in SAR images and they are easily distinguishable from the undisturbed snow surrounding the debris (Vickers *et al.*, 2017).

The manual identification of avalanches based on expert interpretation is a widespread approach reported in the literature, and researchers agree that it still is the golden standard process (Bianchi et al., 2021). However, it has two major limitations, i.e., an expert is needed to locate avalanche debris, and manual identification is subject to observer bias and difficult to reproduce. Another disadvantage is that manual identification can be a very slow process, depending on the size of the investigation area. Since it was not possible to manually locate avalanches for the all 29 SAR image pairs because of the extended size of the investigation area and the limited time availability of an expert, two image-pairs were chosen to be manually investigated. The choice was based on meteorological data, days with intense snowfall were selected and SAR data available immediately before (reference image) and immediately after (activity image) the selected days was used to create an RGB composite. Composite images were created with four different image pairs, i.e., co-polarized VV images and cross-polarized VH images, for both sigma and gamma backscatter, and compared. The composite images were then enhanced using a "standard deviation" stretch type and incrementing the contrast, which allowed for better visualisation of the green tongue-shaped debris. Avalanche debris was then manually delineated, and a vector file created to be used as a mask in the validation process.

Having spent many winter seasons in the mountains professionally as a ski instructor and recreationally as a ski tourer, the author considers his knowledge of avalanches to be sufficient to perform an initial manual identification of avalanche debris. The avalanches that have been identified in the selected SAR images were then double-checked by the expert Dieter Blümel, who is professionally engaged in avalanche prevention and working for the Tyrolean avalanche commission.

Change detection

Avalanche detection is based on temporal change detection of backscatter intensity (Eckerstorfer *et al.*, 2019). Image pairs were created consisting of a reference image that precedes an activity image taken 6 days later. If a new avalanche occurred in the period between the reference image and the activity image, the expected increase in backscatter becomes apparent when subtracting the activity image from the reference image. It is common practice to analyse change detection images so that sudden changes in backscatter become apparent as opposed to stable topographic and land cover features (Wiesmann et al., 2001; Eckerstorfer and Malnes, 2015). In order for change detection to work properly, SAR images with identical imaging geometries must be used (Eckerstorfer, Malnes and Müller, 2017). The image pairs created will be referred to as change detection image pairs.

Since backscatter intensity depends strongly on snow surface characteristics and snow dielectric proprieties, the accuracy of avalanche detection is highly dependable on the net relative backscatter change between the two images used for temporal change detection (Muller *et al.*, 2021). This poses a problem when snow transitions from wet to dry due to meteorological conditions. In those cases, the net backscatter change between the two images is high; however, the relative difference in backscatter between avalanche areas and undisturbed snow remains low.

In order to highlight changes in backscatter and maximise the chance of avalanche identification, different filters were applied to the change detection images and results were compared. Based on literature I decided to test the following options:

A **Low pass** filter that smooths the data by reducing local variation and removing noise. High and low values are averaged out and extreme values in the data are reduced (ESRI, 2022)
A **High pass** filter that accentuates the comparative difference between a cell's values and its neighbours. It highlights boundaries between features and sharpens edges between objects. It is usually employed to correct for large-scale backscatter changes due to wet snow (Leinss *et al.*, 2020).
A **Median** filter that is supposed to reduce noise but preserve edges (Wesselink *et al.*, 2017).
Clipping can be used to normalize backscatter intensity, e.g. the lower and upper 1% on dB values can be clipped (Leinss *et al.*, 2020), or a range can be chosen, such as from -10dB to +10dB, in which avalanches are mostly found (Tompkin and Leinss, 2021).
The **Refined Lee** filter is a de-speckle filter that uses a non square window to match the direction of edges (Esri). It is meant to preserve edges, linear features, and point target and texture information (Filipponi, 2019).

An example of the different filters applied to a selected mapped avalanche is shown in the results section.

Classification

To perform a semi-automatic identification of avalanche debris we must rely on an algorithm's ability to decide whether a change in backscatter should be classified as an avalanche. To perform this classification, different methodological approaches are available. First, the choice is between supervised and unsupervised classification. The aim of this research is to create a model to be tested on semi-regional scale and eventually applied on a regional and possibly even inter-regional scale. If an avalanche database is to be created, all available SAR data from the past winter seasons, from records beginning, must be analysed. For those reasons the model must be as automatised as possible and thus the research focused on unsupervised classification.

The second choice is between **pixel- and object**-based interpretation. Pixel-based is a traditional approach that decides what class each pixel belongs in on an individual basis, whereas the object-based approach (OBIA) groups neighbouring pixels together based on how similar they are in a process known as segmentation, averaging the values of the pixel (Lillesand, Kiefer and Chipman, 2015). One of the most common feature extraction techniques in remote sensing image classification is the OBIA approach (Blaschke 2010), a technique that clusters pixels into objects based on their spectral similarity (Addink and Coillie 2010). The advantages of OBIA are that it reduces the mixed pixels issues which exists in the pixel-based approach (Salehi, Daneshfar, and Davidson 2017), and it allows a straightforward comparison of objects using easy-to-implement algorithms (Chen et al., 2012). Based on that knowledge, the OBIA approach was chosen for this research and iterative self-organising (ISO) data analysis technique was chosen to partition data into clusters, so that cells with similar backscatter values were collected into a group.

An alternative approach to ISO data analysis could be the application of K-means data analysis technique. The main difference between ISO and K-means is that ISO allows the number of clusters created during the iteration process to be adjusted automatically, whereas K-means algorithm determines the number of classes in an early stage, and that number cannot change while the iteration is in progress (Sirat, Setiawan and Ramdani, 2018). Both techniques were tested, and they produced very similar results, which is in line with the literature. Nevertheless, the ISO algorithm was preferred because it did not need the number if clusters to be defined a priori.

Before classification, the mask described in the previous chapter was added, after all four mask layers had been merged in one dataset containing all areas where avalanche detection should not be performed. This allows the classification process to be confined to areas where backscatter values are not heavily distorted/influenced by features such as forests or urban areas, which could negatively influence the classification process.

The results from the classification process underwent visual inspection and class best fit to represent avalanche debris was chosen based on (1) overlap with known mapped avalanches and (2) the highest backscatter values expected from the rough snow surface. This chosen class was subjected to a process of post classification.

Post classification

In this step pixels/cells clusters representing potential avalanche debris accumulation underwent a generalization process aimed at cleaning the data. This was needed because the classification process often results in many isolated small zones of data that are either misclassified or irrelevant to the analysis. This was especially important given the aim to eliminate single pixels that produced noise, and to group pixels with the same backscatter values that were very close to each other, but not adjacent. The generalisation process can be sub-divided into three major steps: 1) Removing the single misclassified cells by replacing them based on most of their contiguous neighbouring cells; 2) Smoothing boundaries so that the smaller zones will invade the larger zones and small groups of cells are integrated with larger ones; and 3) Eliminating clusters that are smaller than a certain threshold. The threshold needs to be chosen with care as this procedure may eliminate useful data.

The generalisation process has the drawback that it may introduce errors in the identification of avalanche debris by distorting the original shapes of the cells clusters oversimplifying them and by eliminating the possibility to detect smaller avalanches.

Validation process

The output of the semi-automatic detection model was validated against mapped avalanches, and against avalanches manually detected by an expert in both investigation regions. The validation was performed for the two selected dates when high avalanche activity was expected after heavy snowfall.

Only for the Trentino region, where mapped avalanches with date stamp where unavailable, I applied a different validation methodology. The mapped avalanches were used to identify areas of high avalanche probability knowing that it is generally assumed that the avalanche events in the future will predominantly repeat themselves in the documented avalanche regions (Hebertson and Jenkins 2003). Therefore, if a SAR detected avalanche debris is within the boundaries of a previously mapped avalanche it is assumed that the detection has a higher probability of being correct compared to events detected outside the mentioned boundaries.

Polygons representing semi-automatically detected avalanches were overlaid with mapped avalanches, and, in a second step, with manually detected avalanches. An analysis was performed to determine the degree of overlap of the two layers and to produce statistics.

Results

Masks

The creation of the **avalanche runout zone** mask posed some challenges. The calculation of PRA (Potential Release Areas), needed as input for the calculation of the avalanche runout zones, was tested on a small subset of the data (with an area of approximately 200 km^2) and produced good results, however the script took a long time to execute. Testing the algorithm on the whole dataset (3,640 km2) resulted in an execution time that was inestimable. For that reason, the process was aborted in favour of a simpler approach that did not make use of PRA. Instead, a slope calculated from a DEM was used, where only inclinations with a gradient between 30° and 60° were extracted. Based on Buhler (2018), a slope between 30° and 60° is where avalanche release is expected. The avalanche runout zones, i.e., areas where avalanche debris can be expected, represent 78.8% of the whole investigation area.

The slope mask that excluded terrain steeper than 35° was adjusted to 30° to limit the false detection of avalanche debris found especially on steep slopes near ridges. In these areas it is very likely for avalanches to be triggered, but far less likely for avalanche debris to accumulate.

Layover and shadow areas that were excluded from the analysis covered 1,218 km2. In the southern part (Trentino region), this amounts to 37.3% of the investigation area. Whereas in the northern part of the investigation area shadow and layover amounts to 30.8 % of the total surface. Figure 7 shows, in green, the shadow and layover mask and how strongly it can affect the exploitability of the SAR data. This becomes particularly apparent in the highlighted areas A and B. The area within the blue dotted line (A) shows how layover and shadow is strongly present along the border of the investigation area. This part is characterised by a continuous shadow and layover coverage rather than more localized patches visible elsewhere. This artefact creates a continuous shadow and layover stripe that entirely covers sections of the investigation area. The red extent indicator (B) points to the specific mountain range called Brenta Group. It is characterized by dolomitic rock formations featuring particularly high and steep mountains. Here shadow and layover areas are more extended than in the rest of the image.

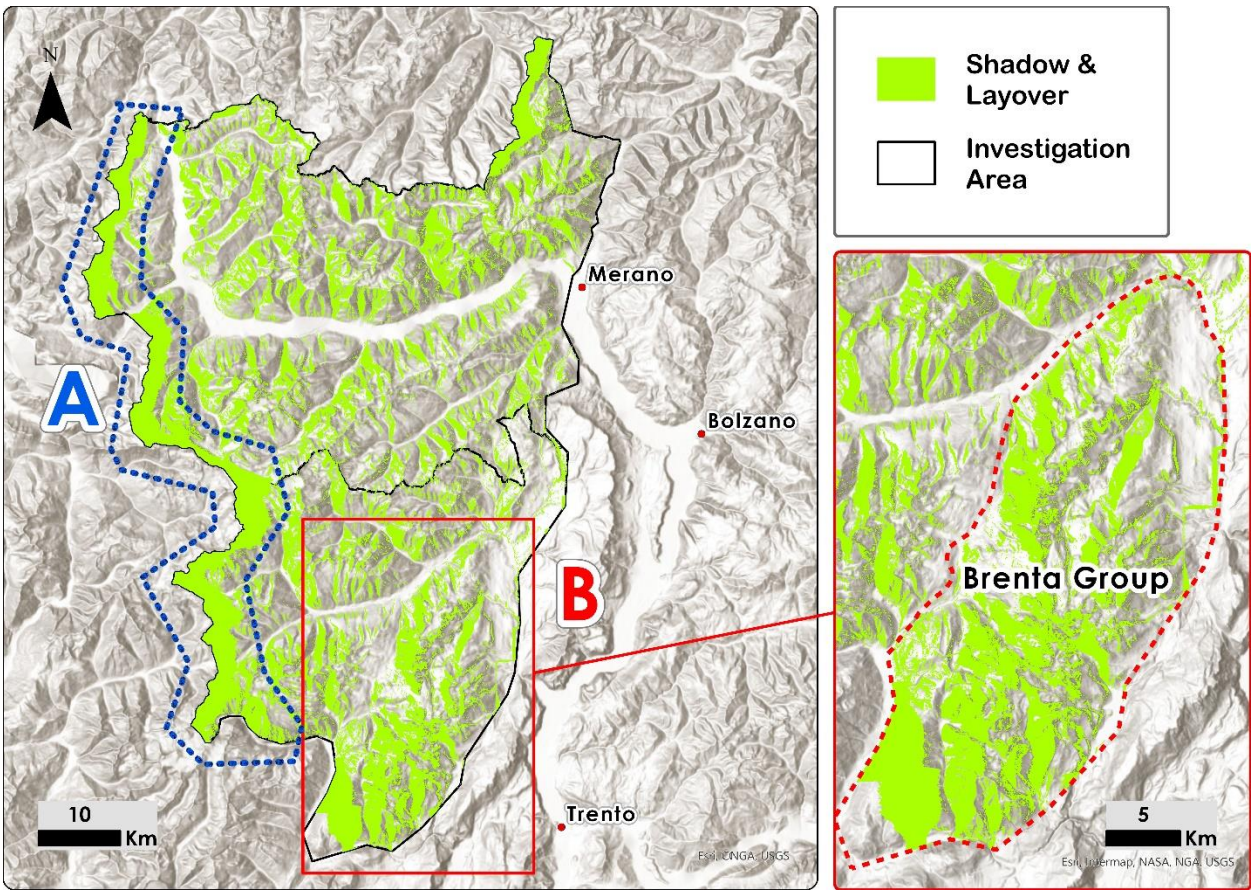

Figure 7: In green area of shadow and layover. (A) highlights the western border of the investigation areas where areas of shadow and layover are widespread to a greater extent. (B) shows a detail of a mountain group (Brenta) with particularly high and steep mountainous formations.

Cumulatively, the applied masks produced a surface of 2,777 km2 to be excluded from the analysis, which corresponds to 76.2% of the investigation area. More specifically, 43.7% of the investigation area is covered by forests, water bodies or urban areas, 33.4 % is shadow or layover, and 21.1% lies outside avalanche runout zones (Figure 8). The areas covered by the mentioned masks overlap in some cases, e.g., it can happen that shadow and layover areas are found within a forest and fall naturally outside an avalanche runout zone. For that reason, superposing the three masks results in a surface which is less than the sum of the three masks' areas.

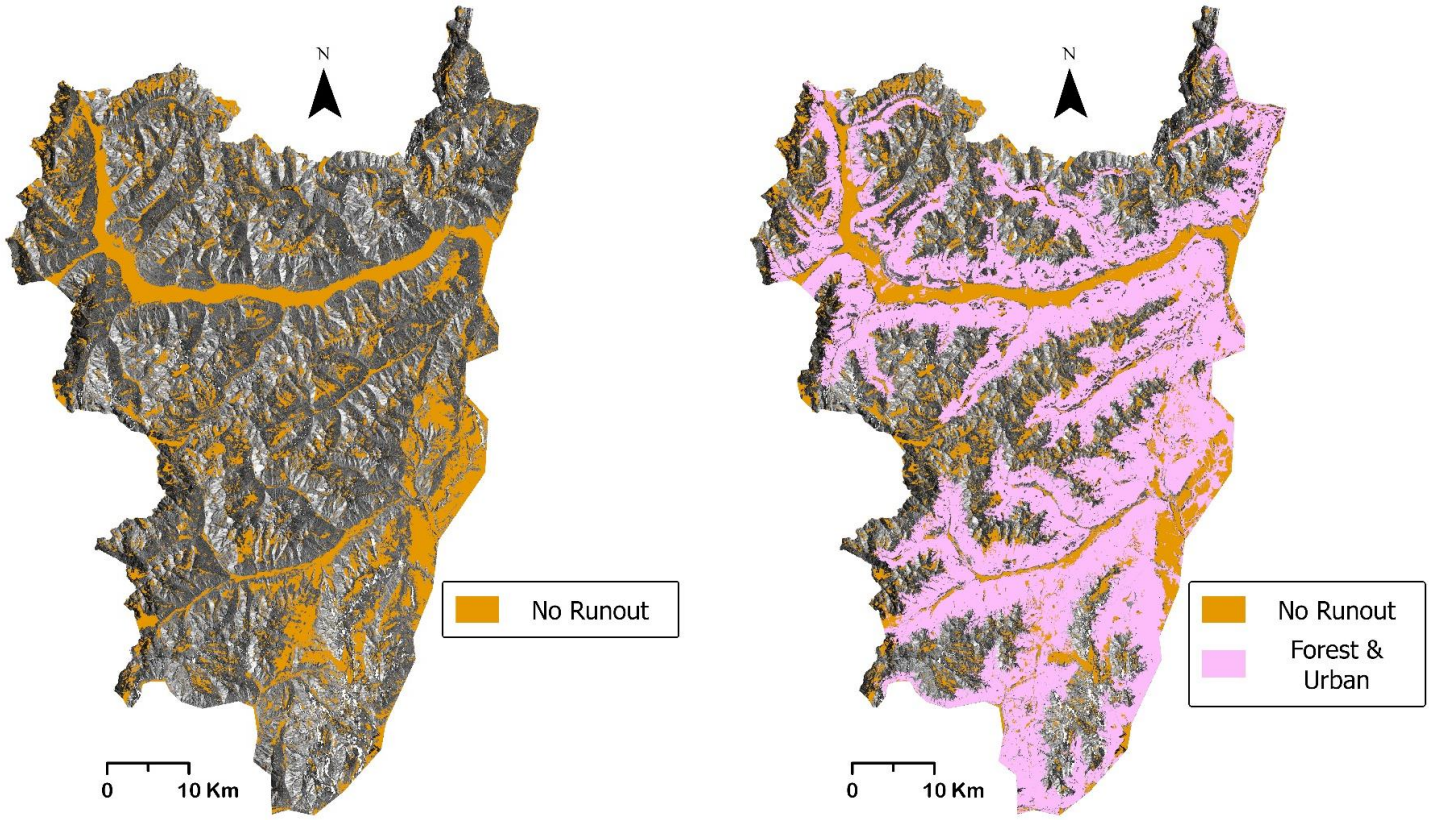

Figure 8: (Left) areas that fall outside avalanche runout zones (No Runout) are excluded from analysis together with (right) forested and urban areas.

Change detection

Change detection is performed on SAR data resulting from subtracting the reference image from the activity image, i.e., the change detection image. The application of different filtering and de-speckling techniques applied to this product produced varying results of image enhancement that influenced the visibility of cell clusters with similar values. The results of these different filters applied to the change detection image are shown in Figure 9. The mapped Sattel avalanche was taken as reference to visualize whether changes in backscatter values are visible in the expected zone of deposition (circled in yellow). The first map series shows results from VH polarized SAR data, whereas Figure 10 shows the application of the same filters on VV polarized SAR data. The clipping technique that was tested to normalize backscatter intensity did not return any useful results in enhancing the visibility of avalanche debris and will therefore not be shown in the example below.

Finally, the refined Lee filter was chosen, defining the window size parameter as 7x7 cells. Upon visual inspection of change detection image pairs de-speckled with this type of filter, it appears that known avalanche debris areas result with higher visibility and slightly better-defined borders. This is confirmed by literature, e.g. by Filipponi (2019), who states that the **refined Lee** filter is superior, compared to other speckle filters, for visual interpretation, because of its ability to preserve edges, linear features, and point target and texture information. (Filipponi, 2019)

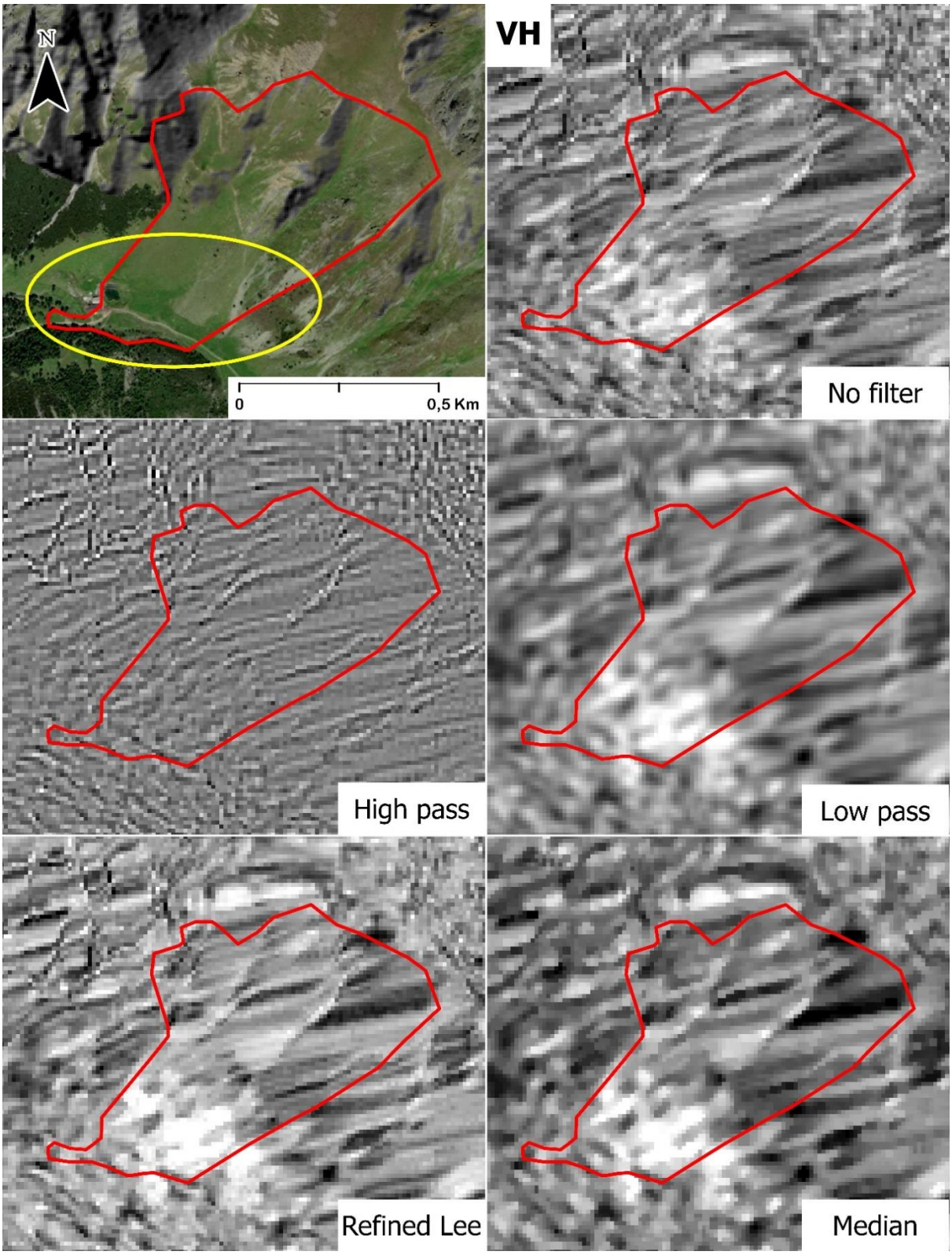

Figure 9: Map series showing (top left) the mapped Sattel avalanche in red with the expected zone of deposition in yellow; (top right) the change detection image created from VH polarisation; (centre left) application of a high pass filter; (centre right) application of a low pass filter; (bottom left) application of a refined lee filter; (bottom right) application of a median filter.

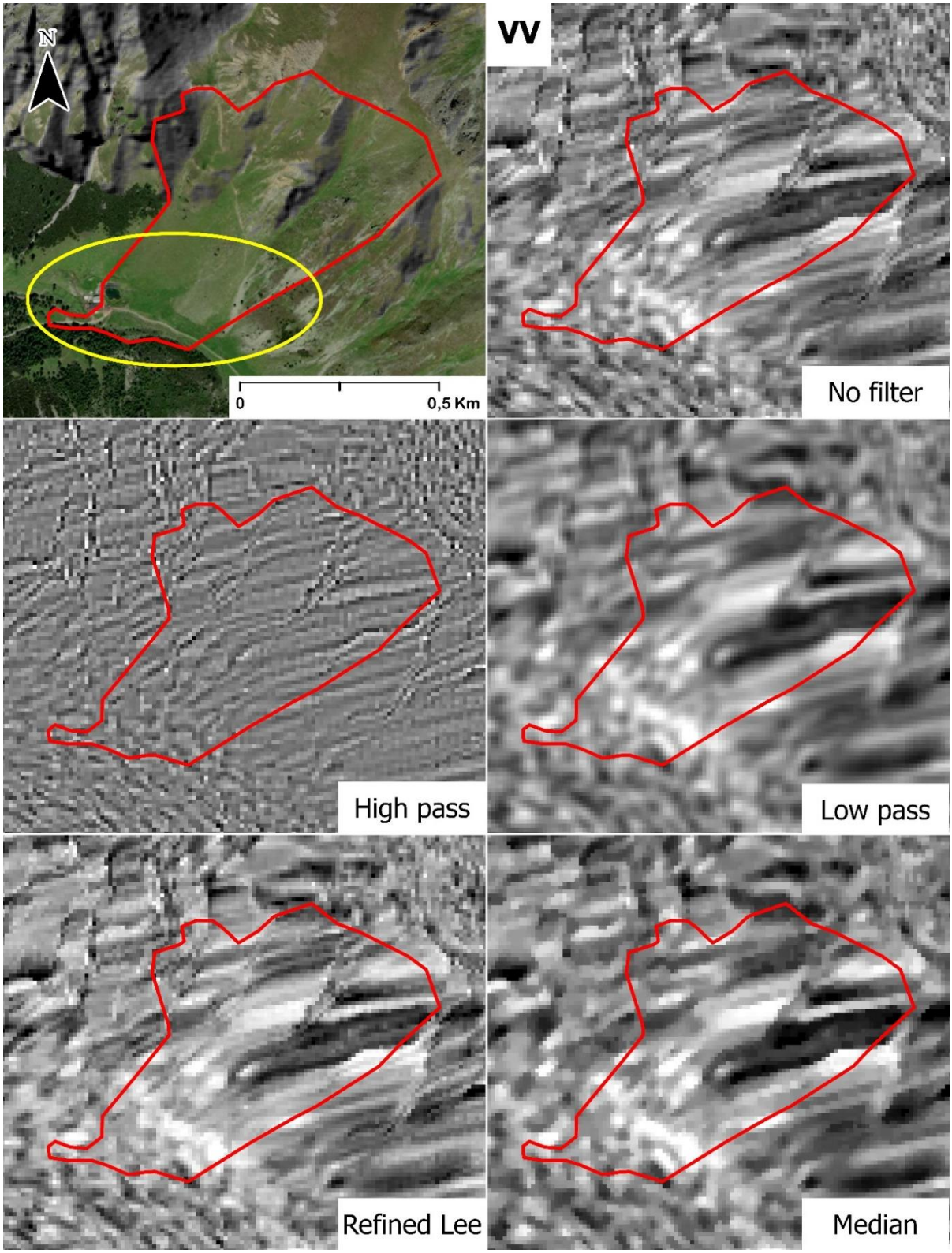

Figure 10: Map series showing (top left) the mapped Sattel avalanche in red with the expected zone of deposition in yellow; (top right) the change detection image created from VV polarisation; (centre left) application of a high pass filter; (centre right) application of a low pass filter; (bottom left) application of a refined lee filter; (bottom right) application of a median filter.

Semi-automatically detected avalanches

The results of SAR semi-automatically detected avalanche debris zones were sub-divided into three sections. First, general results of all detected avalanches from all image pairs will be presented. Next, results are compared to mapped avalanches, and then to manually identified avalanches.

For an avalanche detection from SAR data to be considered successful, some identification criteria must first be defined. When SAR detected avalanche debris covers less than half the surface of the lower third part of a mapped avalanche, the detection is considered partial (Figure 11). If the SAR detected avalanche debris covers more than half of the mentioned surface, the detection is considered total (Figure 12). Rarely cells originating from the proposed detection method entirely cover the expected zone of deposition of an avalanche. This can be due to errors originating form imprecise measuring during the mapping process of an avalanche, or from the masked-out areas that sometimes protrude into zones of deposition.

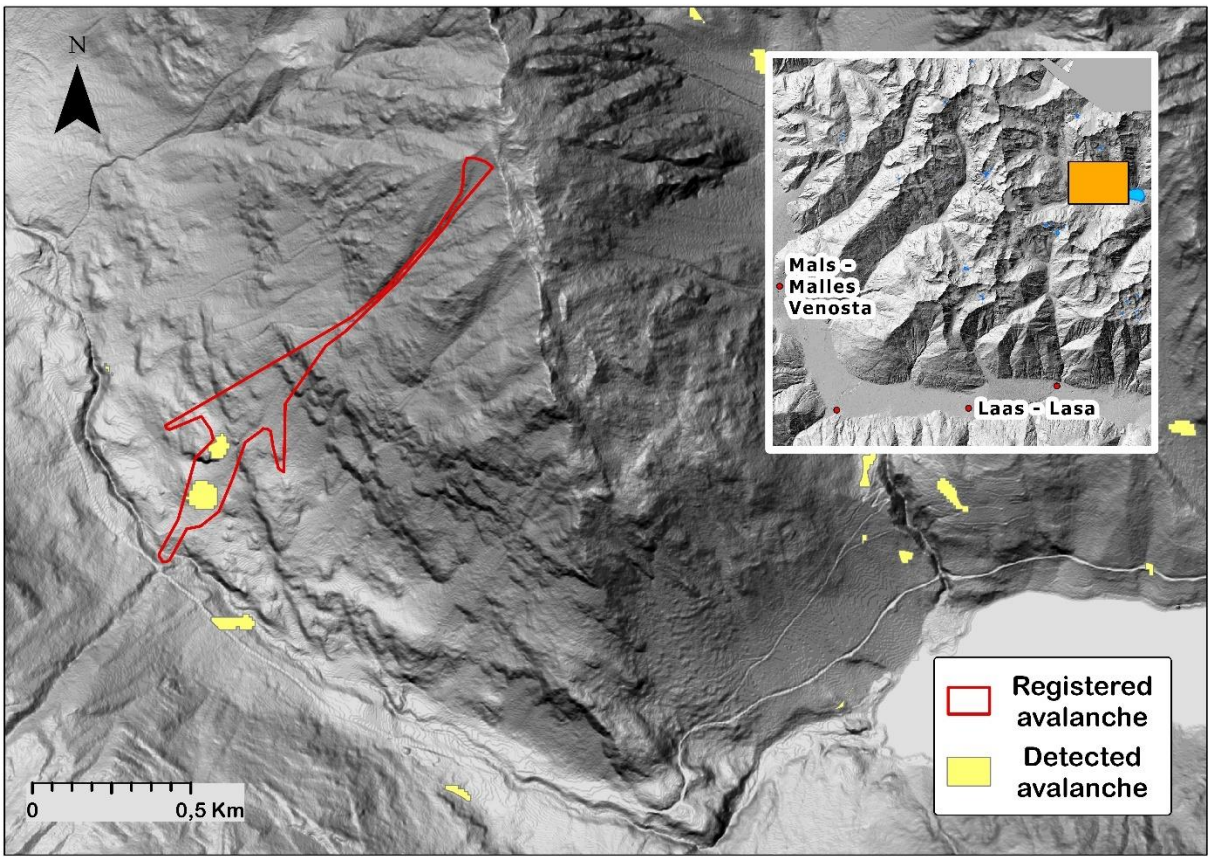

Figure 11: An avalanche event dating from 25.01.2018 in the upper Schnals valley (South Tyrol) that was partially detected using SAR data. The detected avalanche debris (yellow) cover less than 50% of the expected zone of deposition, making this a partially detected avalanche.

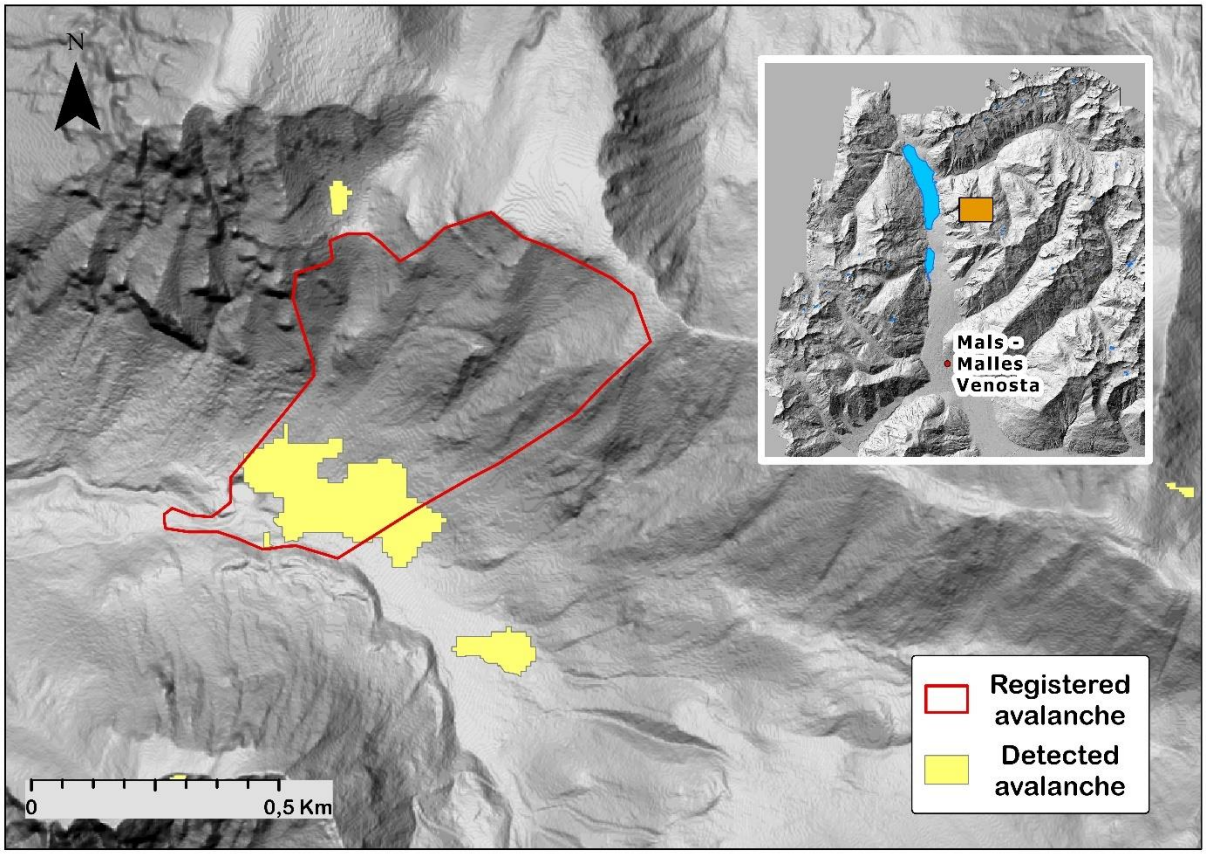

Figure 12: An avalanche event dating from 25.01.2018 in the upper Schnals valley (South Tyrol) that was partially detected using SAR data. The detected avalanche debris (yellow) cover less than 50% of the expected zone of deposition, making this a partially detected avalanche.

Excluded data

Some SAR data did not contain any useful information for avalanche detection. This was due to a late winter season start with very little snowfall before 05/12/2017; therefore, SAR data acquired before that date was not analysed. All together six SAR acquisition dates were eliminated: Table 5 shows the detailed information.

Table 5: SAR scenes deleted due to the lack of avalanche events caused by the absence of a relevant snow cover.

Nr.	SAR data (file names)	Acquisition Date
1	S1A_IW_GRDH_1SDV_20171102T170650_20171102T170715_019089_0204A4_**4D2C**	02/11/2017
2	S1B_IW_GRDH_1SDV_20171108T170607_20171108T170632_008193_00E7AB_**483F**	08/11/2017
3	S1A_IW_GRDH_1SDV_20171114T170650_20171114T170715_019264_020A1A_**F4ED**	14/11/2017
4	S1B_IW_GRDH_1SDV_20171120T170607_20171120T170632_008368_00ED01_**6542**	20/11/2017
5	S1A_IW_GRDH_1SDV_20171126T170650_20171126T170715_019439_020FA4_**80C2**	26/11/2017
6	S1B_IW_GRDH_1SDV_20171202T170606_20171202T170631_008543_00F27E_**F5CB**	02/12/2017

All detected avalanches

Table 6 presents the number of detected avalanche debris for every day when a new SAR scene was available, sub-divided into detections obtained using VV polarisation and detections obtained using VH polarisation. It is to be noted that a partial avalanche detection can be made of several patches of avalanche debris classified cells, as is exemplified in Figure 11. In those cases, the avalanche is one, however the detection scheme identifies two or more patches of debris for the same avalanche. The numbers in Table 6 are not to be considered as detected avalanches per se, but rather as debris accumulation zones. Accordingly, the total number of detected avalanche debris patches presented in Table 6 is not to be considered equal to the number of detected avalanches, as one avalanche can often be mapped with several patches of debris.

Table 6: Detected avalanche debris patches for every SAR scene, sub-divided into VV polarisation and VH polarisation.

Date	***Detected VV***	***Detected VH***
14/12/2017	4795	4261
20/12/2017	3024	-
26/12/2017	4629	3017
01/01/2018	11463	7545
07/01/2018	4693	3969
13/01/2018	4921	5738
19/01/2018	4639	3769
25/01/2018	4313	4816
06/02/2018	4749	5251
12/02/2018	3090	2361
18/02/2018	5209	4661
24/02/2018	4998	3441
02/03/2018	3783	3415
08/03/2018	4022	3348
14/03/2018	4758	6135
20/03/2018	3767	3382
26/03/2018	5775	7959
01/04/2018	5708	3943
07/04/2018	6747	11041
13/04/2018	5014	2922
19/04/2018	5338	10169
25/04/2018	5768	4032
Average	***4749***	***5008***
Total	**99740**	**105175**

In Figure 13 all avalanches detected during the whole season from co-polarized VV SAR data and from cross-polarized VH SAR data are presented.

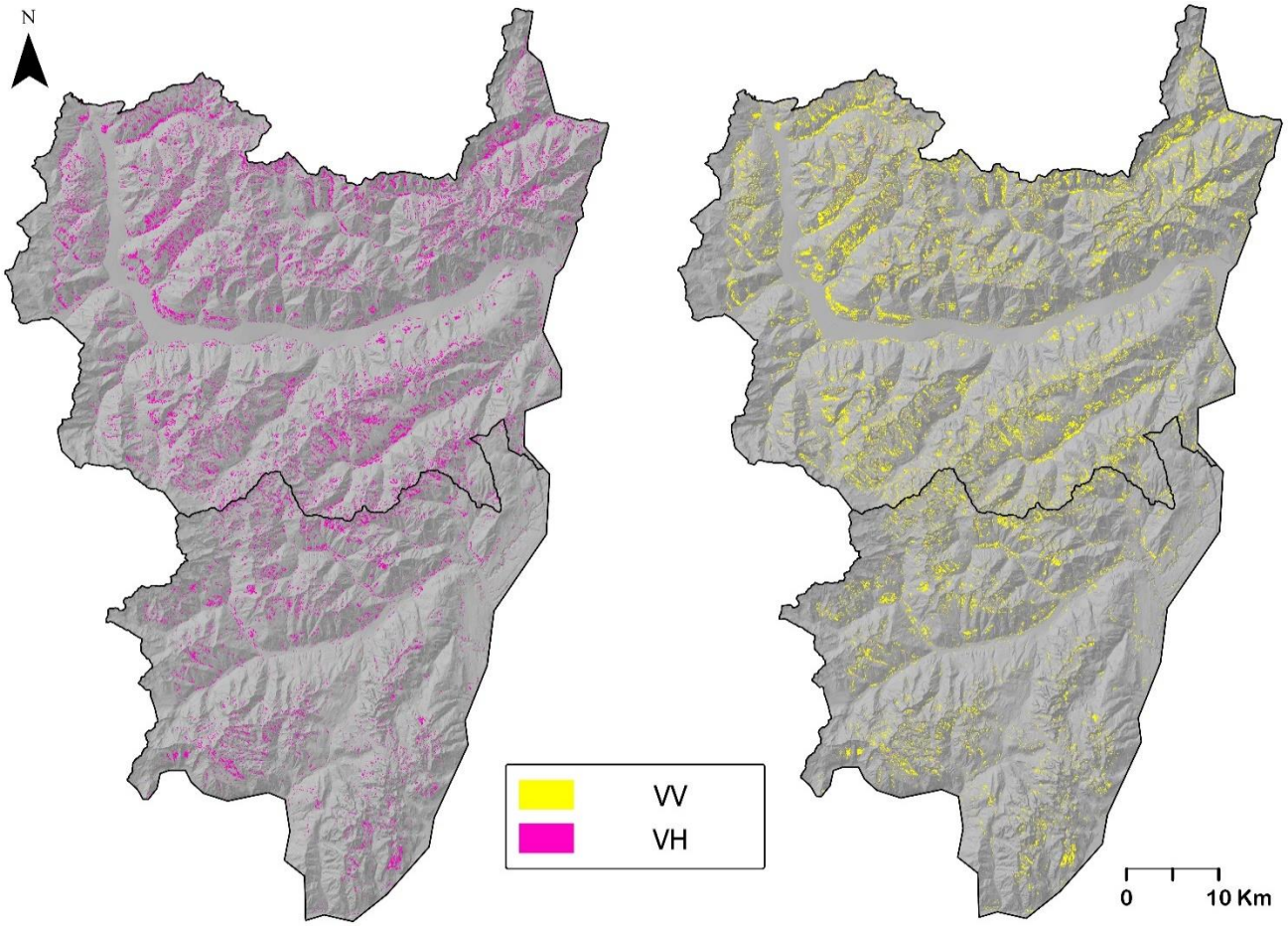

Figure 13: All semi-automatically detected avalanches of the season, sub-divided into detections from co-polarized VV data and cross-polarized VH data.

The area covered by all detected avalanche debris clusters during the whole investigation period corresponds to 322.6 km² for the VH polarisation and 364.6 km² for the VV polarisation. These values should only be considered as a comparison between results obtained with different polarisations.

Comparison with mapped avalanches

Table 7 presents results of correctly detected avalanches based on days when mapped avalanches were available. Those results are limited to the South Tyrol region, since mapped avalanches in the Trentino region miss the indication of a specific occurrence date. The count of detected avalanches refers to, in this example, both partially and totally detected events. On the event date 13/11/2017 no data on detected avalanches is available because the classification procedure produced only two classes, none of which could be assigned to represent avalanche debris.

Table 7: Mapped avalanches on selected days, detected avalanches resulting from the semi-automatic detection method, and rate of correctly detected avalanches.

DATE	MAPPED AVAL	DETECTED AVAL	DETECTED %
13/11/2017	1	No Data	-
03/01/2018	1	0	0
04/01/2018	9	4	44
05/01/2018	1	0	0
06/01/2018	1	1	100
21/01/2018	1	1	100
22/01/2018	24	17	71
23/01/2018	2	2	100
24/01/2018	1	1	100
11/03/2018	1	0	0
31/03/2018	1	0	0
01/04/2018	4	4	100
17/04/2018	2	0	0
TOTAL	49	30	**62.5%**

Figure 14 shows how many of the 49 mapped avalanches were partially detected and totally detected. Counting both partial and total detections as positively identified avalanches, a detection rate of 62.5% is reached. Missed avalanches tend to be located within or very close to forested areas, or they are elongated in shape and very narrow in the zone of deposition. The limits imposed by the resolution of the Sentinel-1 SAR data make it impossible to detect small ground features.

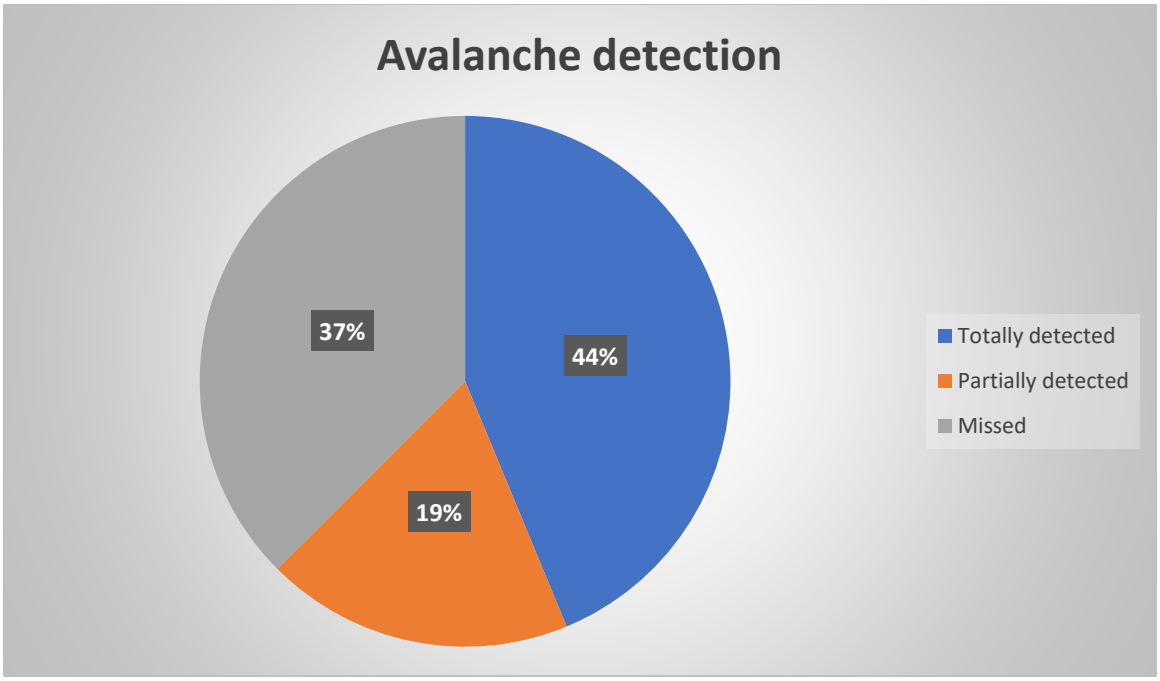

Figure 14: Out of all mapped avalanches on the selected date, 44% were totally detected using SAR data, 19% were partially detected, and 37% were missed.

Comparison with manually detected avalanche debris

Manual avalanche detection was performed for two selected days, 25/01/2018 for the South Tyrol region, and 14/01/2017 for the Trentino region. Results are presented comparing manually detected avalanches with semi-automatically detected avalanches for those two selected dates only. In this case no distinction is made between total or partial detection since no exact mapping of the zone of deposition is available when it comes to manually detected avalanche debris.

Table 8 shows the total number of manually detected avalanches resulting from the first identification performed by the author, and the number of detected avalanches that were confirmed by expert analysis. Respectively 93% and 90% of the initially detected avalanches were confirmed by the expert, whereas the remaining were declared dubious and thus excluded from the selection.

Table 8: Number of avalanches manually detected by the author, and number of avalanches confirmed by the expert.

Avalanches	**South Tyrol**	**Trentino**
Manually detected	60	65
Confirmed by expert	56	59

Table 9 shows how many events were detected, missed, and the resulting detection rate using manually detected avalanches as reference.

Table 9: Avalanches that were correctly detected with the semi-automatic approach compared with manually mapped avalanches from SAR RGB composite images.

AVALANCHES	SOUTH TYROL	TRENTINO
Manually detected and confirmed	56	59
Sem-automatically detected	47	47
Missed	9	12
Detection rate	**83.9%**	**79.6%**

Manual detection of avalanches was performed on the cross-polarisation, sigma nought, VH image composite. Tests were performed in order to manually detect avalanches in sigma nought and gamma nought RGB image composites. Sigma nought produced images with better contrast and avalanches debris could be more easily identified compared to gamma nought. Furthermore, co-polarized VV image composites were compared with cross-polarized VH image composites. Figure 15 shows this comparison focusing on a mapped avalanche where debris is expected in the lower third part of the red polygon. This example event, called Sattel avalanche, will be used often to present other results as well. It is a mapped avalanche that was registered on the 22/01/2018, and it was a particularly large one, measuring 660 m in width and 950 m in length. Its size produced a large amount of snow masses that accumulated in the zone of deposition, making it highly visible within SAR data. Furthermore, its location is favourable for SAR detection as it lies completely over the treeline, and it is not affected by shadow or layover.

The left image shows the mapped avalanche with a satellite snow-free image as basemap; in the centre is the RGB composite in the VH polarisation, and on the right the RGB composite in the VV polarisation.

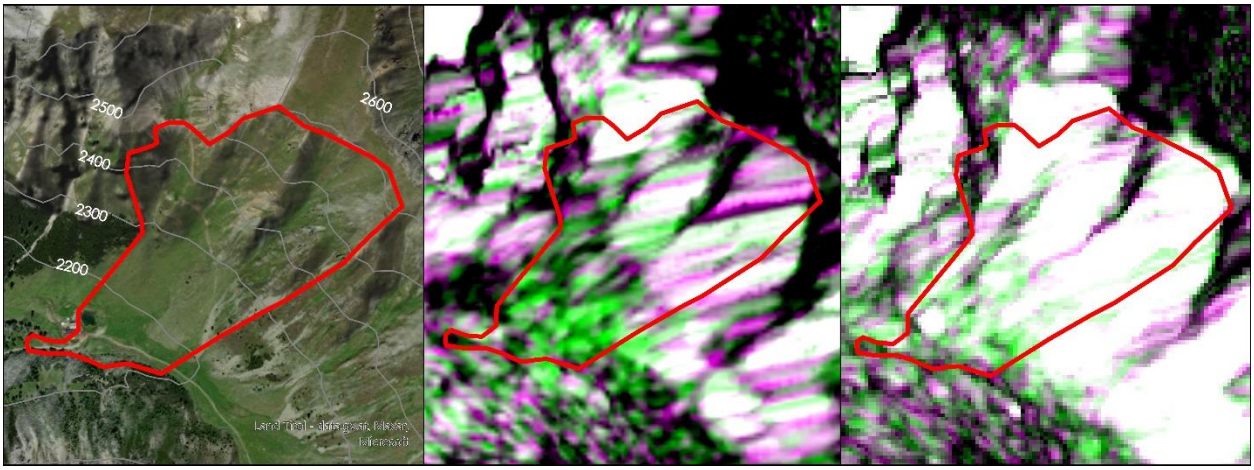

Figure 15: The boundaries of a mapped avalanche (left), RGB image composite showing in green increased backscatter values in VH polarisation (centre), and in VV polarisation (right).

Manual avalanche debris detection was performed on specific days were avalanche activity was expected to be high after heavy snowfall. Based on the knowledge that precipitation was

differently distributed in the two investigation regions, the manual inspection of two different image pairs was performed.

The first image pair, consisting of a reference image from 19/01/2018 and an activity image from 25/01/2018 was created for the South Tyrol region. The unique meteorological situation in the South Tyrol region during January 2018 requires a detailed analysis. Heavy snowfall distributed on the whole region in the first half in January produced fresh snow accumulation of up to 162 cm, the highest value ever locally registered. On the 22/01/2018 temperatures began to rise considerably causing snowfall to turn into rain up to 2000 m above sea level (Weather South Tyrol, 2022b). The combination of these two factors i.e., extraordinary snow accumulation and sudden temperature rise, produced an ideal environment for avalanche formation, such that the local avalanche prevention authority issued a bulletin for 23/01/2018 of avalanche risk at level 5 (very high), which is extremely rare.

The second image pair chosen consisted of the reference SAR scene from 08/12/2017, and the activity SAR scene from 14/12/2017. Between 11/12/2017 and 12/12/2017, 67 cm of new snow were registered in the meteorological station of Folgarida, in the Trentino region. Therefore, the choice fell on comparing SAR data acquired shortly before and SAR data acquired shortly after those two days.

False positives

In this section an example of avalanche debris that were considered potential false positives are presented. To detect false positives a visual inspection of the detected avalanche debris was performed on small, selected areas. The criteria used to define whether detected debris is realistic or not were based on the location and shape of the detection. The analysis was performed using a hillshade or a satellite image as basemap in conjunction with contour lines to better understand the terrain's slope. Figure 16 shows a red polygon representing SAR detected avalanche debris in an uncommon location. In fact, approximately 50 m uphill from the red polygon to the left, a forested area can be seen which acts as a natural barrier for avalanches. Furthermore, between the forested area and the avalanche debris polygon, the terrain presents a slight inclination of approximately 5°, which is too flat for an avalanche to be triggered. Lastly, the red polygon lies on agricultural land, where often higher SAR backscatter values are registered. For the mentioned reasons, the exemplified avalanche debris detection is to be considered a false positive.

Quantifying the rate of total false positives in the investigation area was not possible due to the nature of the inspection approach. In fact, visual analysis is a slow process that can hardly be performed on the whole investigation area. However, to get an approximated estimate of possible false positives, an analysis was performed concerning the overlap of detected avalanche debris with agricultural land. Results show that on average, for every SAR image, 15% of detected avalanche debris is found on agricultural surfaces. Not all SAR detected avalanches over agricultural land can be categorized as false positives; however, the likelihood that increased backscatter values are caused by factors different from avalanche debris is high.

In some cases, avalanche debris is found on ground that presents low- to no sloping. In some cases, those detections are to be considered as false positives. However, avalanche debris can in fact also be found on flat ground if the location is in proximity of steeper ground. The calculation of avalanche runout zones serves exactly this purpose, namely, to differentiate flat ground areas where avalanche debris can be found from flat areas where avalanche debris is unlikely due to the distance from steep slopes.

Figure 16: Avalanche debris polygon likely to be a false positive.

Discussion

The results show that a correct detection rate of avalanche debris from SAR data ranging from 62% to 80% can be achieved on selected dates where avalanche activity is expected to be high due to meteorological conditions. The proposed model confirms that avalanche debris detection is possible in the investigation area with a correct detection rate that is in line with the literature. In fact, results obtained from other studies that use change detection for the identification of avalanche debris reach a correct detection rate of 70% (Leinss et al., 2020), 60% (Vickers et al., 2016), 79% (Eckerstorfer et al., 2019) and 57% (Muller *et al.*, 2021).

The main difference of the proposed approach is the intervention rate required by the user that remains as low as possible. Other studies rely on defining a backscatter threshold above which snow is classified as rough and can be considered avalanche debris. This threshold is different for every SAR image and needs to be adapted manually. The proposed semi-automatic approach, however, does not make use of the thresholding technique that necessitates user intervention in form of parameter definition. This could lead to a higher number of false positives, in the meantime keeping the method more automated. The idea was to produce a model that can be operational on its own, making it independent from user expertise or knowledge. The only parameters required in the proposed semi-automatic avalanche debris detection scheme are those necessary for the ISO clustering step. However, results presented in this study were obtained exclusively applying the software's pre-set values, i.e., minimum class size 20; sample interval 10.

It is to be noted that other avalanche identification techniques such as colour-based detection methods (Karas et al., 2022), or machine learning approaches (Bianchi et al., 2021), have, in general, a similar correct detection rate of respectively 70% and 66%, compared to change detection approaches. However, those require training data and can thus not be considered semi-automatic.

The implications of this research underline the applicability of spaceborne avalanche monitoring using SAR data to be used to create avalanche danger zones that directly originate from known avalanche events, instead of inferring danger based on other parameters such as slope, aspect, or meteorological data. Furthermore, the research highlighted the need for data concerning the spatio-temporal distribution of past avalanches that is, at present, limitedly available to local authorities.

An unexpected outcome of this research comes from the comparison of the VV and VH polarisations used to detect avalanche debris. While it is usually expected that VH polarisation is more sensitive to changes in surface roughness, it was observed that this was not always the case. In fact, VH images reveal avalanche debris with better accuracy when it comes to large avalanches that create large areas of accumulation. However, medium sized avalanches are detected with similar accuracy in VV and VH images, and VV polarisations often detects small avalanches that are missed by the VH polarisation. Within the framework

of this research, it was not possible to determine whether the detection of small avalanches from VV polarized images were true positives or false detections. In total, VV images produced the detection of 99,740 avalanche debris polygons that span a surface of 364.6 km^2, whereas VH images produced 105,175 polygons with a total surface of 322.6 Km^2. In the VH images, slightly more avalanche debris areas are found that are generally smaller compared to those identified in VV polarisation images.

Limitations

The analysis also revealed some limitations in avalanche detection as described in more detail below. For each limiting factor an improvement proposal is defined that could address the shortcoming in future research.

False negatives

Two interacting factors may have caused avalanche debris to be missed by SAR based detection: (1) Sentinel-1 sensors characteristics and (2) ground target characteristics. The C-band operating Sentinel-1 sensor with its wavelength of approximately 6 cm is not able to penetrate dense vegetation, and the tree canopy produces noisy and out of phase SAR data. For those reasons avalanche debris deposited within forest is not detectable. The employment of SAR data with longer wavelength, such as L-band, could solve the problem of missed avalanches within forested areas, which cover a consistent part of the investigation surface (44%). In fact, longer wavelengths have the capability of penetrating vegetation and to be reflected from the ground features underneath the tree canopies. Thus, backscatter values would be representative for possible avalanche debris accumulated within forests. Another sensor characteristic that limits detection capabilities is the side looking nature of SAR, that produces area of shadow and layover. The last sensor characteristic that may lead to missed avalanches is Sentinel-1's resolution of 10 m: ground features smaller than 10 m2 cannot be detected. Accordingly, ground target characteristics, such as size, shape, and location, play a major role in the detection capabilities of any SAR system.

The second cause for false positives is the characteristics of ground targets, such as avalanche size, shape, and location. Avalanche size plays as major role as the 10 m spatial resolution of Sentinel-1 SAR limits the detection of small avalanche debris or debris that is distributed in a thin and elongated shape. Especially wet avalanches, which have in general high surface roughness that facilitates identification in SAR images (Wesselink et al., 2017), are often elongated in shape and thinner in width than 10 m. These events are generally missed in the detection procedure, or not detectable in the first place as they often lie within forested areas that were masked out. Generally speaking, squared to rectangle shaped avalanche debris is more likely to be resolved (Wesselink et al., 2017). With the knowledge that small- or thinner than spatial resolution avalanches cannot be detected, all debris smaller than 40 m^2 could, in future, be eliminated from the results. Small avalanches can be

considered of minor importance in this study, as they are generally unable to bury a person and can thus be considered less dangerous (Eckerstorfer *et al.*, 2019). Higher spatial resolution SAR data could be investigated to address the size issue. **Location** of avalanches is another limiting factor when it comes to avalanche debris detection, especially considering areas of radar shadow and layover, which cover 33% of the investigation area, or forested areas. To limit shadow and layover SAR data acquisitions from orbits with opposite view directions (ascending, looking east, and descending, looking west) could be used by combining the backscatter values using a weighted average from the two datasets (Leinss *et al.*, 2020). This would optimize spatial resolution and minimise shadow and layover effects.

False positives

Given the high number of semi-automatically detected avalanche debris, and having carefully visually inspected some selected areas, it appears clear that false positives are present in the results. It is difficult to quantify their exact number because visual inspection cannot be performed on the whole investigation area. However, three major indicators have been identified, that help determining the possibility of an avalanche detection to be incorrect, i.e., the position, the type of surface were debris was found, and meteorological conditions leading to the event. The position reveals that some detected avalanches appear to be located just below of forested areas. Those detections are dubious because avalanche deposition can hardly be found downhill of dense forest where avalanches cannot penetrate, except for small avalanches triggered just below the treeline. For that reason, avalanche debris in proximity, and downhill from forested areas is to be considered as a possible false positive. A solution for those misinterpretations would be the creation of a more sophisticated mask. Specifically, for the calculation of the potential release area (PRA) of an avalanche, additionally to slope and terrain curvature, parameters of land cover type could be included. However this is not a straightforward task, and several studies are addressing this topic as a whole research area on its own (Sykes, Haegeli and Bühler, 2022).

The type of **surface** covered by the snow can be the second indicator pointing to a false positive. The most evident example is agricultural land, that is characterized by a high sensitivity to surface roughness changes (Eckerstorfer *et al.*, 2019), and can lead to high SAR backscatter values caused by factors different from avalanche debris. Furthermore, agricultural land is usually situated at lower altitudes where snow melt can be faster, thus exposing bare soil to the radar signal. From C-band SAR it is not possible to distinguish whether the ground is covered with dry snow or no snow at all (Eckerstorfer, Malnes and Müller, 2017). Further analysis should be performed to determine on which specific type of agricultural land false positives most often occur, in order to then mask out those areas. Another surface that was considered liable to produce false positives due to its sensitivity to snow cover changes is in glaciers. However, it was found that avalanche debris is rarely detected on perennial glaciated surfaces. The reason could be attributed to the relatively

gentler slopes found on glaciers, and the fact that less steep ground is present above glaciers where avalanches could be triggered.
The third cause for false detection is when snow is transformed from wet to dry due to **meteorological** conditions. In those cases, change detection performed on two SAR images will present values of highly increased backscatter in the activity image, because of the increased level of humidity in the snow, and not because of increased surface roughness produced by avalanche debris. In fact, the largest backscatter contribution in dry snow is from the ground (Wesselink et al., 2017). However, when snow is transformed from wet to dry, the snow-pack tends to consolidate, thus the days that present those specific meteorological conditions could be excluded from analysis as avalanches can generally be ruled out then (Tompkin and Leinss, 2021).

Reference data

Reference data to be employed as ground truth was more difficult to find or produce than initially thought. The reasons are mainly two: (1) officially registered and mapped avalanches are few and are often located in areas where SAR data in unavailable or unreliable; and (2) manual detection of avalanche debris from RGB composites is a laborious task that could hardly be accomplished for the whole investigation area in the reference period. Two approaches have been identified that could, in future research, maximise the exploitability of the available reference data: (1) limit the investigation area and period to the availability of reference data; (2) employ high resolution optical imagery to confirm detected avalanches. Focusing the analysis on smaller areas where more avalanches have been mapped, and on specific days where avalanche activity was high over many winter seasons, could prove useful. In fact, reference data for this study in the South Tyrol region was made of 49 mapped avalanches; however, if different areas and periods had been chosen, 200 mapped avalanches would have been available as reference data. Consequently, it would be easier to obtain high resolution optical data, e.g., from the SPOT6 satellite with a resolution of 1.5 m, if smaller regions and specific periods were selected, as this kind of data needs to be especially requested. However, higher resolution does not necessarily lead to better results, as it is shown by Hafner et al. (2020), who compared avalanche debris detection from optical SPOT6 data and Sentinel-1 SAR data, finding that “the probability of the existence of an avalanche according to the ground truth, is nearly the same”, based on positive predictive values (PPV). SPOT6 data produced a PPV of 0.88, and Sentinel-1 data a PPV of 0.87. In conclusion, a robust avalanche database can be constructed and used as reference data if the contribution of residents and mountain enthusiasts is channelled toward a systematic acquisition of images and descriptions of avalanche events every time someone witnesses one. An example of this can be found in Switzerland and is described by Hafner et al. (2020): people in the mountains witnessing avalanches can easily report them through an online application.

In addition to being scarce, available reference data is not always accurate. Mapped avalanches are usually outlined using optical images as reference, and an accurate measurement does not take place. Therefore, incongruence between SAR detected debris and mapped avalanches is possible.

Conclusion

The faculty to monitor avalanche activity with continuity throughout an entire winter season in a selected region is essential for avalanche forecasting and hazard mapping. This research attempted to assess the applicability of avalanche debris detection in the western part of the Italian region of Trentino-Alto Adige, from spaceborne Sentinel-1 SAR data using a semi-automatic approach. The outcome of this research primarily consists in areas of semi-automatically identified avalanche debris that were compared to known avalanches that have been mapped and to manually detected avalanches resulting from expert interpretation. Only a fraction of the detected avalanches could be compared to validation data due to the limited availability of mapped avalanches and the difficulties to create a dataset of manually detected avalanches. The vast majority of detected events can therefore not be confirmed with certainty. Only a visual interpretation (manual approach) performed by an expert can estimate the veracity of each avalanche, mainly based on its location in relation to slope and landcover. However, the scope of the study was the creation of a semi-automatic detection scheme that needs as little manual intervention as possible. Furthermore, the manual validation of avalanche debris on such a large dataset was not feasible within the framework of the research. Results, however, are positive since between 70% and 80% of detected avalanches were confirmed when compared to manually detected avalanches on two selected eventful dates. Furthermore, 62% percent of detected avalanches were confirmed when compared to mapped avalanches. These results are in line with recent literature, and higher correct detections rates can only be achieved using neural networks and the application of training data. This answers one of the research questions that was defined in the introduction, i.e., can SAR data be applied to detect avalanche debris in the investigation area, and with what accuracy. Regarding the research question concerning which avalanche size can best be detected, it was confirmed that medium to large size avalanche debris can best be delectate, whereas avalanche debris smaller than approximately 40 m^2 is mostly missed due to the resolution of Sentinel-1 data. The last research question aimed at identifying which SAR polarization returns best results could not be answered with certainty. In fact, VH polarized images that are expected to return best results when identifying avalanche debris, produced better results only in cases of large avalanches. With medium sized avalanches, VV and VH images produce very similar results. VV polarisation could be more accurate in identifying small avalanches, however, this could not be confirmed during the research.

The main weakness of the proposed model is the over detection and the presence of false positives. This, and other minor issues, still need to be addressed before the model can become operational. Automation of the proposed model reached a satisfactory level; however, human intervention is still needed to perform all the processing steps. The time needed to perform the whole process, from querying SAR data to the output of a binary map containing snow avalanche debris polygons, is about 25 minutes. Reaching a level of total automatization is desirable and can realistically be achieved by merging the pre-processing part, currently performed within the SNAP software, into the ArcGIS Pro environment, as

well as creating a shell script that automatically downloads new selected SAR scenes whenever available, as proposed by Eckerstorfer et al. (2019).

Once the model if refined, mainly addressing the improvements proposed in the discussion section, and once the automation is complete, the application on other research areas and periods can be implemented. This would soon create a consistent database of past avalanche events and a plethora of new opportunities of statistical analysis of avalanche events could be initiated.

Outlook

Currently avalanche risk zones are defined based on a sophisticated risk exposure analysis based on elements such as slope, aspect, surface type and land cover. Past avalanche events are also taken into consideration; however, these carry a limited weight as data is scarce. Knowing that avalanche events in the future will mainly re-occur in the documented avalanche regions (Hebertson and Jenkins, 2003), integrating the information of all avalanches of the past winter seasons (starting from 2014 with the first availability of Sentinel-1 SAR data) would lead to a solid improvement of avalanche risk zone definition.

Over the course of this research the author has been in contact with the main regional departments of avalanche forecast and prevention to discuss procedures and obtain useful data. From those interactions, it has become apparent that the results of this research would be warmly welcomed by the mentioned authorities, who are experiencing a shortage in data regarding occurred avalanches.

The free availability of remotely sensed data to the public is a great asset for all future research, and ESA's Copernicus programme with its Sentinel satellites is a great example of that. An exciting piece of news is the current development of a new product, the Normalised Radar Backscatter (NRB), designed to be a high-quality-Analysis Ready Data (ARD) (European Space Agency, 2022b), which in the future could be also employed for avalanche debris detection, making analysis easier and more efficient.
The limited selection of freely available SAR data is a major disadvantage, especially considering the possibility of the highly advanced Sentinel satellites malfunctioning. An example of that was seen in December 2021, when the satellite Sentinel-1b experienced a malfunction of the C-band synthetic aperture radar antenna power supply unit that engineers were unable to rectify. The end of the Sentinel-1b mission was announced in August 2022. A new Sentinel-1c satellite launch is targeted before the end of 2023 (ESA, 2022). Until then, the availability of SAR data from the Copernicus programme is limited to Sentinel-1a's products.

In some regions of Norway a model similar to the one proposed is already operational (Eckerstorfer *et al.*, 2019). It helps local authorities to verify the avalanches risk assessment of the previous day and acts as advisor to increase or decrease the momentary avalanches

danger level. This approach could be implemented in the investigation region applying a refined version of the proposed model.

Finally, alternative approaches to the identification of avalanche debris form SAR data are being examined, with recent publications pointing to deep learning methods yielding improved detection results. Further research is required to test neural networks on Sentinel-1 images to detect avalanches on a pixel scale.

References

Alaska Satellite Facility (2022) 'How to View Radiometrically Terrain-Corrected (RTC) Images in ArcGIS'. Available at: https://asf.alaska.edu/how-to/data-recipes/how-to-view-radiometrically-terrain-corrected-rtc-images-in-arcgis/ (Accessed: 1 June 2023).

ASF (2022) 'ASF Data Search Vertex'. Available at: https://search.asf.alaska.edu/#/ (Accessed: 10 March 2022).

Bertschinger, T. (2022) 'Automated mapping of potential snow avalanche release areas (PRAs)'. Available at: https://github.com/unibe-geodata-modelling/2018-snow-avalanches-sources (Accessed: 15 November 2022).

Bianchi, F.M., Grahn, J., Eckerstorfer, M., Malnes, E. and Vickers, H. (2021) 'Snow Avalanche Segmentation in SAR Images With Fully Convolutional Neural Networks', *IEEE Journal of Selected Topics in Applied Earth Observations and Remote Sensing*, 14, pp. 75–82. Available at: https://doi.org/10.1109/JSTARS.2020.3036914.

Buhler, Y., Hafner, E. and Techel, F. (2021) 'Mapping avalanches with satellites - the vision of more complete avalanche datasets', in *2021 IEEE International Geoscience and Remote Sensing Symposium IGARSS*. *IGARSS 2021 - 2021 IEEE International Geoscience and Remote Sensing Symposium*, Brussels, Belgium: IEEE, pp. 232–235. Available at: https://doi.org/10.1109/IGARSS47720.2021.9553577.

Bühler, Y., Hüni, A., Christen, M., Meister, R. and Kellenberger, T. (2009) 'Automated detection and mapping of avalanche deposits using airborne optical remote sensing data', *Cold Regions Science and Technology*, 57(2–3), pp. 99–106. Available at: https://doi.org/10.1016/j.coldregions.2009.02.007.

Bühler, Y., von Rickenbach, D., Stoffel, A., Margreth, S., Stoffel, L. and Christen, M. (2018) 'Automated snow avalanche release area delineation – validation of existing algorithms and proposition of a new object-based approach for large-scale hazard indication mapping', *Natural Hazards and Earth System Sciences*, 18(12), pp. 3235–3251. Available at: https://doi.org/10.5194/nhess-18-3235-2018.

Chawla, M. and Singh, A. (2021) *A data efficient machine learning model for autonomous operational avalanche forecasting*. preprint. Landslides and Debris Flows Hazards. Available at: https://doi.org/10.5194/nhess-2021-106.

Chen, G., Hay, G.J., Carvalho, L.M.T. and Wulder, M.A. (2012) 'Object-based change detection', *International Journal of Remote Sensing*, 33(14), pp. 4434–4457. Available at: https://doi.org/10.1080/01431161.2011.648285.

Choubin, B., Borji, M., Mosavi, A., Sajedi-Hosseini, F., Singh, V.P. and Shamshirband, S. (2019) 'Snow avalanche hazard prediction using machine learning methods', *Journal of Hydrology*, 577, p. 123929. Available at: https://doi.org/10.1016/j.jhydrol.2019.123929.

Congedo, L. (2023) 'Semi-Automatic Classification Plugin'. Available at: https://plugins.qgis.org/plugins/SemiAutomaticClassificationPlugin/ (Accessed: 12 February 2022).

Dostalova, A., Navacchi, C., Greimeister-Pfeil, I., Small, D. and Wagner, W. (2022) 'The effects of radiometric terrain flattening on SAR-based forest mapping and classification', *Remote Sensing Letters*, 13(9), pp. 855–864. Available at: https://doi.org/10.1080/2150704X.2022.2092911.

EAWS (2023a) 'European Avalanche Warning Services'. Available at: https://www.avalanches.org/ (Accessed: 11 December 2022).

EAWS (2023b) 'European Avalanche Warning Services. Fatalities'. Available at: https://www.avalanches.org/fatalities/ (Accessed: 15 December 2022).

Eckerstorfer, M., Bühler, Y., Frauenfelder, R. and Malnes, E. (2016) 'Remote sensing of snow avalanches: Recent advances, potential, and limitations', *Cold Regions Science and Technology*, 121, pp. 126–140. Available at: https://doi.org/10.1016/j.coldregions.2015.11.001.

Eckerstorfer, M. and Malnes, E. (2015) 'Manual detection of snow avalanche debris using high-resolution Radarsat-2 SAR images', *Cold Regions Science and Technology*, 120, pp. 205–218. Available at: https://doi.org/10.1016/j.coldregions.2015.08.016.

Eckerstorfer, M., Malnes, E. and Müller, K. (2017) 'A complete snow avalanche activity record from a Norwegian forecasting region using Sentinel-1 satellite-radar data', *Cold Regions Science and Technology*, 144, pp. 39–51. Available at: https://doi.org/10.1016/j.coldregions.2017.08.004.

Eckerstorfer, M., Vickers, H., Malnes, E. and Grahn, J. (2019) 'Near-Real Time Automatic Snow Avalanche Activity Monitoring System Using Sentinel-1 SAR Data in Norway', *Remote Sensing*, 11(23), p. 2863. Available at: https://doi.org/10.3390/rs11232863.

ESA (2022) 'Mission ends for Copernicus Sentinel-1B satellite'. Available at: https://www.esa.int/Applications/Observing_the_Earth/Copernicus/Sentinel-1/Mission_ends_for_Copernicus_Sentinel-1B_satellite (Accessed: 13 December 2022).

ESRI (2022) 'Technical Support'. Available at: https://support.esri.com/en-us/overview (Accessed: 20 March 2023).

Euregio, E. (2022) 'Avalanche report'. Available at: https://avalanche.report/bulletin/latest (Accessed: 1 August 2023).

European Space Agency (2022a) 'Definitions'. Available at: https://sentinel.esa.int/web/sentinel/user-guides/sentinel-1-sar/definitions (Accessed: 20 January 2022).

European Space Agency (2022b) 'Sentinel Online'. Available at: https://sentinel.esa.int/web/sentinel/home (Accessed: 23 January 2023).

Filipponi, F. (2019) 'Sentinel-1 GRD Preprocessing Workflow', in *3rd International Electronic Conference on Remote Sensing*. *International Electronic Conference on Remote Sensing*, MDPI, p. 11. Available at: https://doi.org/10.3390/ECRS-3-06201.

Flores, A., K. Herndon, Rajesh Thapa and Emil Cherrington (2019) 'Synthetic Aperture Radar (SAR) Handbook: Comprehensive Methodologies for Forest Monitoring and Biomass Estimation'. Available at: https://doi.org/10.25966/NR2C-S697.

Giffard-Roisin, S., Sinha, S., Karbou, F., Deschatres, M., Karas, A., Eckert, N., Coléou, C. and Monteleoni, C. (2020) *Detecting avalanche debris from SAR imaging: a comparison of convolutional neural networks and variational autoencoders*. other. pico. Available at: https://doi.org/10.5194/egusphere-egu2020-9487.

Hebertson, E.G. and Jenkins, M.J. (2003) 'Historic climate factors associated with major avalanche years on the Wasatch Plateau, Utah', *Cold Regions Science and Technology*, 37(3), pp. 315–332. Available at: https://doi.org/10.1016/S0165-232X(03)00073-9.

Karas, A., Karbou, F., Giffard-Roisin, S., Durand, P. and Eckert, N. (2022) 'Automatic Color Detection-Based Method Applied to Sentinel-1 SAR Images for Snow Avalanche Debris Monitoring', *IEEE Transactions on Geoscience and Remote Sensing*, 60, pp. 1–17. Available at: https://doi.org/10.1109/TGRS.2021.3131853.

Keiler, M., Zischg, A., Fuchs, S., Hama, M. and Stötter, J. (2005) 'Avalanche related damage potential - changes of persons and mobile values since the mid-twentieth century, case study Galtür', *Natural Hazards and Earth System Sciences*, 5(1), pp. 49–58. Available at: https://doi.org/10.5194/nhess-5-49-2005.

Kumar, S., Narayan, A., Mehta, D., and Snehmani (2022) 'Snow cover characterization using C-band polarimetric SAR in parts of the Himalaya', *Advances in Space Research*, 70(12), pp. 3959–3974. Available at: https://doi.org/10.1016/j.asr.2022.10.012.

Leinss, S., Wicki, R., Holenstein, S., Baffelli, S. and Bühler, Y. (2020) 'Snow avalanche detection and mapping in multitemporal and multiorbital radar images from TerraSAR-X and Sentinel-1', *Natural Hazards and Earth System Sciences*, 20(6), pp. 1783–1803. Available at: https://doi.org/10.5194/nhess-20-1783-2020.

Lillesand, T.M., Kiefer, R.W. and Chipman, J.W. (2015) *Remote sensing and image interpretation*. Seventh edition. Hoboken, N.J: John Wiley & Sons, Inc.

McClung, D.M. (2002) 'The Elements of Applied Avalanche Forecasting, Part II: The Physical Issues and the Rules of Applied Avalanche Forecasting', *Natural Hazards*, 26(2), pp. 131–146. Available at: https://doi.org/10.1023/A:1015604600361.

Meteotrentino (2022) 'Dati e osservazioni'. Available at: https://www.meteotrentino.it/index.html#!/home (Accessed: 14 January 2023).

Muller, K., Eckerstorfer, M., Grahn, J., Malnes, E., Engeset, R., Humstad, T. and Widforss, A. (2021) 'Norway's Operational Avalanche Activity Monitoring System Using Sentinel-1', in *2021 IEEE International Geoscience and Remote Sensing Symposium IGARSS*. *IGARSS 2021 - 2021 IEEE International Geoscience and Remote Sensing Symposium*, Brussels, Belgium: IEEE, pp. 236–238. Available at: https://doi.org/10.1109/IGARSS47720.2021.9553152.

Provincia Autonoma di Trento (2023) 'WebGIS'. Available at: https://webgis.provincia.tn.it/wgt/?topic=1&lang=it&bgLayer=sfondo&layers=ammcom,cv_direttrici,DTMSol315&layers_visibility=false,true,true&X=5114686.98&Y=666632.01&zoom=7&catalogNodes=6,18 (Accessed: 2 July 2021).

Schweizer, J., Bruce Jamieson, J. and Schneebeli, M. (2003) 'Snow avalanche formation: AVALANCHE FORMATION', *Reviews of Geophysics*, 41(4). Available at: https://doi.org/10.1029/2002RG000123.

Sinha (2019) 'Can Avalanche Deposits be Effectively Detected by Deep Learning on Sentinel-1 Satellite SAR Images?'

Sirat, E.F., Setiawan, B.D. and Ramdani, F. (2018) 'Comparative Analysis of K-Means and Isodata Algorithms for Clustering of Fire Point Data in Sumatra Region', in *2018 4th International Symposium on Geoinformatics (ISyG)*. *2018 4th International Symposium on Geoinformatics (ISyG)*, Malang: IEEE, pp. 1–6. Available at: https://doi.org/10.1109/ISYG.2018.8611879.

Small, D. (2011) 'Flattening Gamma: Radiometric Terrain Correction for SAR Imagery', *IEEE Transactions on Geoscience and Remote Sensing*, 49(8), pp. 3081–3093. Available at: https://doi.org/10.1109/TGRS.2011.2120616.

Suedtiroler Buergernetz (2023) 'GeoKatalog'. Available at: http://geokatalog.buergernetz.bz.it/geokatalog/#! (Accessed: 20 December 2022).

Sykes, J., Haegeli, P. and Bühler, Y. (2022) 'Automated snow avalanche release area delineation in data-sparse, remote, and forested regions', *Natural Hazards and Earth System Sciences*, 22(10), pp. 3247–3270. Available at: https://doi.org/10.5194/nhess-22-3247-2022.

Tarboton, D. (2023) 'Terrain Analysis Using Digital Elevation Models (TauDEM)'. Available at: https://hydrology.usu.edu/taudem/taudem5/ (Accessed: 5 January 2023).

Tarboton, D.G. (1997) 'A new method for the determination of flow directions and upslope areas in grid digital elevation models', *Water Resources Research*, 33(2), pp. 309–319. Available at: https://doi.org/10.1029/96WR03137.

Tedesco, M. (ed.) (2015) *Remote Sensing of the Cryosphere*. 1st edn. Wiley. Available at: https://doi.org/10.1002/9781118368909.

Tompkin, C. and Leinss, S. (2021) 'Backscatter Characteristics of Snow Avalanches for Mapping With Local Resolution Weighting', *IEEE Journal of Selected Topics in Applied Earth Observations and Remote Sensing*, 14, pp. 4452–4464. Available at: https://doi.org/10.1109/JSTARS.2021.3074418.

Vickers, H., Eckerstorfer, M., Malnes, E. and Doulgeris, A. (2017) 'Synthetic Aperture Radar (SAR) Monitoring of Avalanche Activity: An Automated Detection Scheme', in P. Sharma and F.M. Bianchi (eds) *Image Analysis*. Cham: Springer International Publishing (Lecture Notes in Computer Science), pp. 136–146. Available at: https://doi.org/10.1007/978-3-319-59129-2_12.

Vickers, H., Eckerstorfer, M., Malnes, E., Larsen, Y. and Hindberg, H. (2016) 'A method for automated snow avalanche debris detection through use of synthetic aperture radar (SAR) imaging: Automated Avalanche Detection', *Earth and Space Science*, 3(11), pp. 446–462. Available at: https://doi.org/10.1002/2016EA000168.

Weather South Tyrol (2022a) 'Daily values for temperature and precipitation'. Available at: https://meteo.provincia.bz.it/download-dati.asp (Accessed: 14 February 2023).

Weather South Tyrol (2022b) 'Publikationen'. Available at: https://wetter.provinz.bz.it/publikationen.asp?publ_page=3 (Accessed: 16 January 2023).

Wesselink, D.S., Malnes, E., Eckerstorfer, M. and Lindenbergh, R.C. (2017) 'Automatic detection of snow avalanche debris in central Svalbard using C-band SAR data', *Polar Research*, 36(1), p. 1333236. Available at: https://doi.org/10.1080/17518369.2017.1333236.

Wiesmann, A., Mätzler, C. and Weise, T. (1998) 'Radiometric and structural measurements of snow samples', *Radio Science*, 33(2), pp. 273–289. Available at: https://doi.org/10.1029/97RS02746.

Wiesmann, A., Wegmuller, U., Honikel, M., Strozzi, T. and Werner, C.L. (2001) 'Potential and methodology of satellite based SAR for hazard mapping', in *IGARSS 2001. Scanning the Present and Resolving the Future. Proceedings. IEEE 2001 International Geoscience and Remote Sensing Symposium (Cat. No.01CH37217)*. *IGARSS 2001. Scanning the Present and Resolving the Future. Proceedings. IEEE 2001 International Geoscience and Remote Sensing Symposium*, Sydney, NSW, Australia: IEEE, pp. 3262–3264. Available at: https://doi.org/10.1109/IGARSS.2001.978322.

Yang, J., Li, C., Li, L., Ding, J., Zhang, R., Han, T. and Liu, Y. (2020) 'Automatic Detection of Regional Snow Avalanches with Scattering and Interference of C-band SAR Data', *Remote Sensing*, 12(17), p. 2781. Available at: https://doi.org/10.3390/rs12172781.